Taylor & Francis
Taylor & Francis Group

Drying Technology
An International Journal

ISSN: (Print) (Online) Journal homepage: https://www.tandfonline.com/loi/ldrt20

Experimental analysis of spray drying in a process intensified counter flow dryer

Umair Jamil Ur Rahman, Artur K. Pozarlik & Gerrit Brem

To cite this article: Umair Jamil Ur Rahman, Artur K. Pozarlik & Gerrit Brem (2021): Experimental analysis of spray drying in a process intensified counter flow dryer, Drying Technology, DOI: 10.1080/07373937.2021.2004160

To link to this article: https://doi.org/10.1080/07373937.2021.2004160

Published online: 08 Dec 2021.

DRYING TECHNOLOGY
https://doi.org/10.1080/07373937.2021.2004160

Experimental analysis of spray drying in a process intensified counter flow dryer

Umair Jamil Ur Rahman, Artur K. Pozarlik, and Gerrit Brem

Thermal Engineering, Department of Thermal and Fluid Engineering, University of Twente, Enschede, the Netherlands

ABSTRACT

This research presents an experimental analysis of a counter flow spray drying process using water and skim milk as a feed. The study was performed by examining the droplet size distribution of sprays and the temperature profiles in the dryer. The influence of air inlet temperature, air mass flow rate, feed flow rate, and droplet size on air temperatures in the dryer was evaluated. The evaporation and deposition zones were found to be highly dependent on the droplet size. The obtained results show that it is possible to achieve efficient contact between hot air and spray in a small volume using a counter-current mechanism.

ARTICLE HISTORY
Received 10 March 2021
Revised 7 October 2021
Accepted 4 November 2021

KEYWORDS
Counter-current spray drying; process intensification; skim milk; droplet size distribution

1. Introduction

Every year, around 2.8 million tons of milk powder is produced in the European Union.[1] This number is likely to increase even further, with the expected increase in food demand by 70% in 2050.[2] The most widely used method for producing dairy powders is spray drying.[3,4] The process involves the atomization of a concentrated liquid feed into tiny droplets that undergo evaporation due to the heat and mass transfer with hot air.[3,5] At present, two kinds of spray dryers are used in the industry, i.e., co- and counter-current dryers.[6,7] For drying of heat-sensitive materials (e.g., milk), co-current spray dryers are used. Here, the feed and hot air enter the reactor from the same direction. The drying paths followed by the droplets in such a configuration limit the maximum air inlet temperatures, thus, limiting the drying rates and overall thermal efficiencies of co-current spray dryers.[4,5,8]

On the other hand, counter-current or mixed flow dryers are used to dry thermally resistant materials (e.g., detergents) by injecting the feed and hot air in the opposite directions.[6,9–11] These dryers intensify the heat and mass exchange as well as the momentum transfer between the droplets and the gas phase. This ultimately results in high thermal efficiencies.[9,12,13]

Spray drying of skim milk in a counter-current configuration is yet to be explored in detail. This is due to the possible degradation of heat-sensitive products since the already dried particles are exposed to high-temperature air just before leaving the drying chamber.[6] In this study, we explore this gap by proposing a novel dryer configuration to achieve product-degradation-free counter-current spray drying process.

A numerical study on a counter-current spray drying process for skim milk was recently conducted by Jubaer et al.[14] In order to control forced agglomeration, authors identified different agglomeration zones such as coalescence, agglomeration, or rebound of dried particles, based on the particle's stickiness criterion. Employing the identical geometry configuration as proposed by Jubaer et al.,[14] Razmi et al.[15] developed a 1d model and investigated the influence of the process parameters (inlet temperature, airflow, feed rate, droplet size) on the drying behavior of whole milk.

A counter-current mechanism, while being thermally efficient, can also be used to produce high-quality crystalline particles with superior properties. This was experimentally demonstrated by Shakiba et al.[16] The results showed that with longer residence time and bigger particle sizes, it was indeed possible to achieve in situ crystallization of lactose droplets.

Over the past decades, the introduction of multi-stage spray dryers and the integration of fluidized beds has improved the energy efficiency of skim milk

CONTACT Umair Jamil Ur Rahman u.jamilurrahman@utwente.nl Thermal Engineering, Department of Thermal and Fluid Engineering, University of Twente, Enschede, the Netherlands.

production units.[17] However, there have been no significant advancements in terms of equipment volume reduction or process intensification (increasing capacity or drying rates),[4,8] which are the biggest challenges posed to spray drying industries.[8,18–20] The increasing world population and stricter restrictions on carbon emissions[21] compels food industries to look for novel processes and technologies that are energy-efficient, have better quality, and have lower capital and operating costs.[22]

A trend toward volume reduction by utilizing Super-Heated Steam (SHS) as a drying medium was presented by Frydman et al.[23,24] using an experimentally validated numerical model; authors concluded that higher drying rates and narrower time distribution could be achieved in a smaller volume utilizing SHS as drying medium compared to hot air. Linke et al.[25] compared skim milk powder produced in a small-scale SHS dryer (height of 0.45 m and diameter of 0.2 m) to that produced by conventional co-current driers. A yellow-brownish color product was obtained via SHS, while similar characteristics in terms of morphology and particle sizes were obtained. Lum et al.[26] concluded that skim milk droplets dried in SHS resulted in a sticky product with more wettability compared to particles dried in hot air, attributed to the difference in component migrations. That being said, a superior spray drying technology with commercial viability should possess high drying rates in a small compact volume without adversely affecting product quality.[8] For this reason, in 2018, the Radial Multizone Dryer (RMD) project was initiated,[27,28] aiming toward process intensification by employing vortex chamber technology.[29–31]

In the RMD configuration, hot air enters the chamber axially in the central zone while a cold rotating flow is created by tangential air inlets in the periphery of the dryer. In this fashion, two temperature zones are established: a hot zone in the middle of the vortex chamber and a moderately cold zone on its peripheries. In consequence, the spray drying process in the RMD occurs in two steps: (i) the injected droplets are exposed to hot air temperatures of 300-400 °C for a few milliseconds in a counter flow manner, and (ii) the almost dried particles are rapidly evacuated to the moderately cold temperature zone (80-120 °C) with the help of the strong centrifugal forces generated due to the high-G acceleration of vortex flow.[31–33] By rapid evacuation of dried particles to a colder environment, product degradation is avoided. The two-step process leads to two drying zones: a fast drying zone in the center and a slow drying zone in the periphery of the chamber.

The application of spray drying in the novel RMD was recently demonstrated by Rahman et al.[34] using a numerical approach. The study revealed that by combining high air inlet temperatures (350 °C) and high-G acceleration (200 g), high drying rates with efficient particle separation were achieved while particle residence time was significantly reduced. The study also showed that the majority of the drying took place in the central hot zone of the dryer. The current paper aims to experimentally study the initial spray drying step of this configuration, i.e., the interaction of milk droplets with hot air in an axial counter-flow manner.

The available literature indicates that the investigations on the drying of milk are limited to co-current dryers while that of counter-current dryers is limited to detergents.[6] An extensive study on a counter-current spray dryer was initiated by Zbicinski and Piatkowski.[9] They used Particle Dynamics Analysis (PDA) and Laser Doppler Anemometry (LDA) methods to examine the airflow and droplet evaporation dynamics for maltodextrin feed. The gas and product temperatures were measured using a modified micro-separator device as used by Kieviet and Kerkhof.[35] The results showed a strong dependency of multiple parameters (atomization parameters, nozzle location, and gas temperatures) on the drying performance leading to a narrow range of stable operating parameters and not stable product characteristics. Moreover, the authors found that the degree of agglomeration in the dryer depends on the nozzle distance from the air inlet.

More recently, Wawrzyniak et al.[12] investigated a similar counter-current dryer with swirling airflow for detergent production. Authors related the following process parameters: airflow rate, swirl number, and atomization parameters to the product quality and moisture content. In this study, the use of pneumatic nozzles with different orifices revealed that an increase in the spray Sauter Mean Diameter (SMD) results in an increase of SMD in the final product. In addition to droplet SMD, airflow rate or swirl number was found to be important parameters in controlling the final moisture content of the particle. It was concluded that the low flow rates promote agglomeration with bigger D50 values and higher moisture content, while high flow rates resulted in overdried particles and smaller D50 values.

In another study, Francia et al.[36] elaborately discussed the factors controlling drying rates,

agglomeration, and wall deposits in an industrial counter-current swirl dryer for detergent production. It was found that optimal drying rate and residence time are a function of the nozzle position, i.e., when the nozzle is placed too close to the air inlet, a high particle concentration zone is produced with wet, dried, and semi-dried particles colliding and forming big agglomerates, while when placed too far from the inlet a decrease in drying capacity was observed due to the loss of fines.

For co-current spray dryers, the application of mono-disperse atomizer has shown great potential in improving the energy and process efficiency of industrial milk production units.[37–41] Atuonwu & Stapley[37] suggested that by producing uniform droplet sizes (sizes ten times smaller than the current atomizers) and thereby better controlling the drying process, energy consumption in spray dryers can be reduced by up to 90%. Deventer et al.[38] discussed the advantages of mono-disperse nozzles for atomization of higher viscosity sprays (>50% solids content) to reduce the amount of water to evaporate. Jaskulski et al.[39] developed a Computational Fluid Dynamics model demonstrating significant advantages of generating uniform droplets such as good control over the drying process, superior product quality, and uniform particle sizes. Fischer et al.[40] designed and tested an inline droplet and particle size distribution system using an image analysis technique for improved control over the process. The review by Moejes and Boxtel[41] indicated that mono-disperse droplet generation is the key element in significantly reducing the amounts of fines in the exhaust air leading to the possibility of dehumidification and recirculation of exhaust air.

Kota and Langrish[42] studied the deposition fluxes of skim milk in a co-current spray dryer fitted with a pneumatic nozzle. In their study, the mean diameter of the spray was calculated to be 12 µm, while the temperature of the air and flow rate was 180 °C and 155 kg/h, respectively. The authors found that increasing the feed rate from 0.31 to 1.70 kg/h (at constant feed/air ratio) resulted in maximum deposition fluxes, while the areas prone to deposition remained the same for all feed rates. The maximum deposition occurred on the bottom plates due to the high velocity of the droplets.

By employing the same dryer configuration, Ozmen and Langrish[43] investigated the deposition pattern of skim milk at varying air inlet temperature and liquid feed rates. The authors demonstrated that the highest deposition fluxes were observed when the air temperature was reduced from 230 °C to 170 °C resulting in slow drying rates, which in turn increased the moisture content of the particles. This led to their shift toward the sticky region. A similar trend was observed when the feed rate was increased from 1.4 to 1.8 kg/h. The optimal conditions (air temperature of 230 °C and feed rate of 1.6 kg/h) from the work of Ozmen and Langrish[43] were utilized further by Langrish et al.[44] to compare the deposition fluxes between maltodextrin and skim milk in the same spray dryer setup. The authors found higher deposition rates for skim milk due to its lower glass transition temperature than maltodextrin. However, in general, maximum deposition fluxes were observed at similar locations for both feed materials.

Gianfrancesco et al.[45,46] analyzed the spray drying of water and aqueous maltodextrin in a co-current spray dryer. By comparing different air inlet temperatures and feed rates, the authors proposed a stickiness regime map based on measured air properties (temperature and relative humidity) inside the dryer and related them to the product properties. The results showed that drying was already completed in the top part of the chamber when the air inlet temperature was set to 200 °C, while drying continued in the bottom part of the dryer when the air inlet temperature was lowered to 144 °C. Furthermore, increasing the feed rate resulted in high moisture content of the recovered product due to low air temperature and relative humidity in the dryer. No powder was recovered when the maltodextrin feed rate increased from 1.8 to 3.6 kg/h because a semi-liquid product was stuck on the chamber walls because of incomplete drying. The authors found that maltodextrin (DE12) with higher glass transition temperature is only sticky near the atomizer, while DE21 with lower glass transition might be sticky even further in the chamber.

Sadripour et al.[47] investigated the influence of feed parameters (feed rate, initial solid content, droplet size) on wall deposition of skim milk in a short-tube-type co-current spray dryer employing experimental and numerical methodologies. The results showed that with increasing feed rate or initial solids content, the deposition on the dryer walls increases linearly, while the amount and location of particle deposition on the dryer walls shift downstream with increasing the initial droplet diameter.

In this study, we present experimental research with water and skim milk in a counter-flow dryer. This work aims to analyze the influence of different process parameters, including air temperature, airflow rate, feed flow rate, and droplet sizes, on the evaporation profiles. The mechanism of skim milk drying in a counter-flow reactor is studied using two different

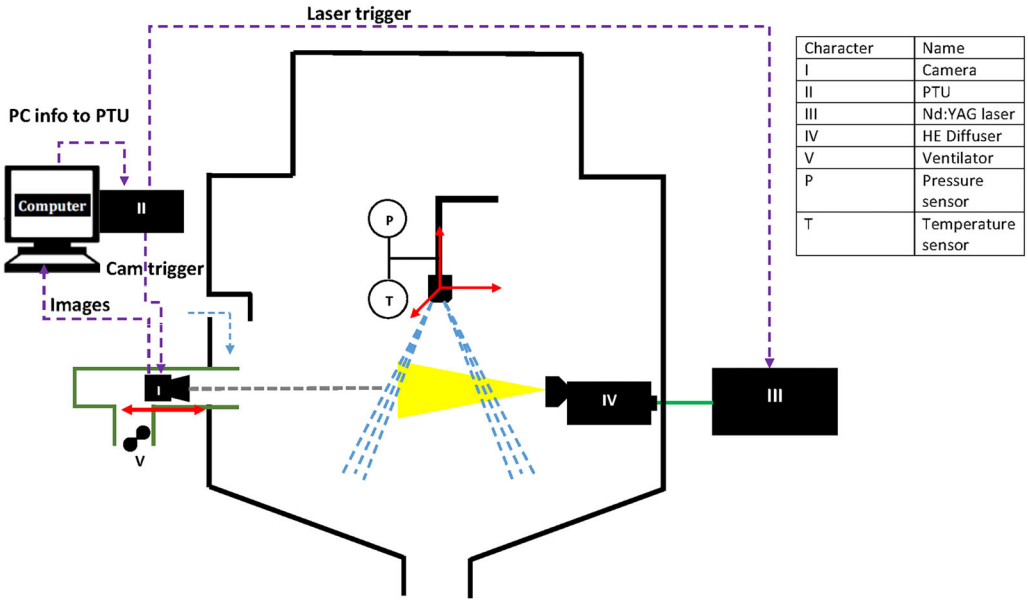

Figure 1. Scheme of the Particle Droplet Image Analysis test-rig.[53]

nozzle orifices. The effects of droplet diameter on the air temperature, along with the deposition pattern and the final product characteristics, are evaluated. This study provides a framework for the two-step drying process in the novel RMD.

2. Experimental methodology

2.1. Particle droplet image analysis (PDIA) setup

The droplet size distribution generated by the atomizers is a crucial factor in spray drying since it controls the drying rates and final particle size distribution. The nozzles employed in this study are centrifugal pressure nozzles that produce a hollow cone spray with 15 degrees angle. They can be characterized by the Flow Number (FN) of approximately 9.10^{-8} m^2 (liquid density = 1000 kg/m^3, liquid pressure = 30 bar). The droplet size measurements are performed in the state-of-the-art atomization test rig operating on a non-intrusive optical method known as Particle Droplet Image Analysis (PDIA).[48–52] The main components of the experimental facility (see Figure 1) are: a double cavity Bernoulli PIV Nd: YAG laser (Bernoulli PIV, Litron Lasers), high-speed camera (SX-9M, LaVision), high light efficiency diffuser, and long-distance microscope (type: Questar QM1 BK7/MgF2 corrector). The droplets from the spray are exposed to a light source generated by Nd: YAG laser. Opposite to the laser, a high-speed camera is located. As the droplets reflect the incident light, they appear as dark spots on the focal plane where the spray measurements take place. The virtual focal plane has a field of view of 5 × 4 mm and a depth of 1 mm. The camera is equipped with a double shutter (inter framing time of 150 ns) and has a resolution of 3360 × 2712 pixels. Furthermore, to have a small field view, an optical microscope with a working range of 56-170 cm and resolution of 3 µm @ 56 cm distance is used. The Nd: YAG laser is capable of generating double pulsed light at a wavelength of 532 nm that enables the application of the Particle Tracking Velocimetry (PTV) to measure droplet velocity.[51,54] The laser has a maximum output of 2 × 200 mJ/pulse with a pulse duration of 4 ns. The timing of the laser pulse and the camera shutter is controlled using a Programmable Timing Unit (PTU). The camera and the laser are fixed while a traverse system is used to move the nozzle position (vertical or horizontal direction) depending on the desired measurement location. In this study, all the measurements are taken at the location of the primary spray breakup. This is to avoid any uncertainty related to the effect of the secondary breakup and to provide a well-defined benchmark for possible CFD research. The primary breakup is defined here, as the location where the Normalized Ligaments Area (NLA), generated by the spray, is below 5% (see equation 1). This parameter is defined as the total area represented by ligaments, normalized with the total surface area of both ligaments and droplets as measured in the images:[52]

$$NLA = \frac{\sum A_{c,lig}}{\sum A_{c,lig} + \sum A_{c,drop}} \quad [1]$$

where A_c refers to the cross-sectional area.

Table 1. Overview of the conditions for droplet size measurements.

Nozzle type	Operating pressure range (bar)	Liquid composition (w/w)		Density (kg/m^3)	Viscosity (mPa-s)
		Water	Glycerin		
Hollow cone pressure nozzle, 15° spray angle	10, 20, 30	100	0	1000	1
		51	47	1118	5
		27	73	1189	30

The feed is pumped to the nozzle using a positive displacement pump (Hydracell G04E, Promotech., UK). The liquid pressure and temperature are recorded before the spray nozzle. The accuracy of the pressure sensors is $\leq$ 0.5%. The raw images are analyzed for droplet size and velocity data using the commercial program Particle Master (DaVis, LaVision). Generally, around 100-200 droplet images are captured to ensure the presence of a statistically large enough number of droplets taken for the analysis. The droplets that are outside the depth of field (1 mm) are removed from the analysis using the procedure described in detail in the work of Lee and Kim.[49] This method uses the Gradient Intensity (GI) parameter to distinguish the droplets that are out of focus. Here, a minimum GI value of 2% and a maximum of 25% were applied to the images. Furthermore, to exclude ligaments/fragments, a minimum centricity filter of 50% was used. Centricity is defined as the ratio of the droplet short axis to the long axis. For the test-rig calibration, a Patterson globe reticle[55] was applied. The measured error was a function of the droplet size and stayed below 12%.

Three hollow cone pressure nozzles with different orifice diameters were researched, i.e., nozzle $1-0.5$ mm, nozzle $2-0.6$ mm, and nozzle $3-0.7$ mm (see for details Table 1). To prevent contamination of the test-rig, a glycerol-water mixture was used as a surrogate for the milk concentrate. Glycerol is commonly used to obtain mixtures with desired physical properties matching the characteristics of the investigated fluid.[52,56,57] The mass percentages of glycerol for the desired viscosities were obtained from the literature, see.[58] Further, the data was confirmed by Klaassen,[59] showing that the difference between the measured viscosity of the glycerol-water mixture and reported data is below 1%.

The droplet size measurements were completed at various liquid viscosities corresponding to the Total Solids (TS) content of milk. Since all the experiments in this study were performed at room temperature of 20 °C, the selected viscosities are slightly higher than the reported viscosities of milk concentrates measured at 55-60 °C.[60,61]

For the measurements, we selected the viscosity of 1, 5, and 30 mPa.s, which are equivalent to a TS content of 0, 20, and 40 wt.%. The viscosity and other liquid properties used for the measurements are shown in Table 1.

2.2. Counter flow dryer setup

Figure 2 illustrates the main components of the experimental facility used for the spray drying experiments. The schematic diagram and visual image of the dryer together with its main dimensions and measurement points are shown in Figure 3a and b, respectively. The dimensions of the drying chamber are chosen to be approximately similar to other vortex chamber studies.[30,32,34,62–64] The main drying chamber has a height of 50 cm and a diameter of 40 cm. The air enters at the bottom via a smaller cylinder that has a diameter of 13 cm and leaves via a centrally positioned exhaust chimney with two gas outlets. The air is heated using 60 kW electric heaters (Roestvrijstaal Industrie) that can heat the air up to 550 °C. The heater temperature is set using a thermostat controller. A pneumatic diaphragm control valve (3730 Samson Regeltechniek B.V.) is used to bring the air into the drying chamber from the main air supply line. The liquid feed is pumped using a positive displacement diaphragm pump (Wanner hydra cell P200), and it is injected using a pressure atomizer at the top of the drying chamber. In this manner, a counter-current configuration is achieved. The feeds, i.e., water and skim, are stored in two separate steel tanks (75-liter volume). Hollow cone centrifugal pressure nozzles (121 V, Schlick., Germany) with varying orifice diameters (see Table 2) are investigated. The produced powder is recovered from the moist air at a cyclone separator. The moist exhaust air goes outside to the atmosphere. The pressure in the drying chamber is slightly above the atmospheric conditions (0,2-0,8 bar(g)). The walls of the dryer are insulated. Four inspection windows (two on the top and two on the bottom wall) are installed in the dryer to visualize the experiments using webcams. The videos were recorded to observe the feed accumulation and droplets impinging or entering the hot air inlet section.

The air temperature was measured using k-type thermocouples (OMEGA Engineering). The error of these thermocouples is $\leq$ 0.5%. The position of the

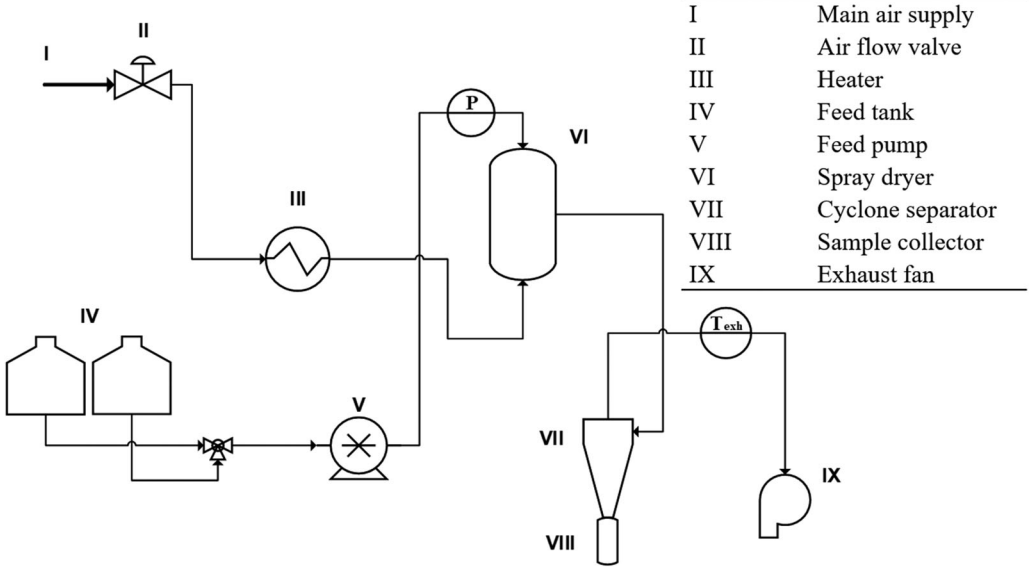

Character	Equipment name
I	Main air supply
II	Air flow valve
III	Heater
IV	Feed tank
V	Feed pump
VI	Spray dryer
VII	Cyclone separator
VIII	Sample collector
IX	Exhaust fan

Figure 2. Schematic diagram of the experimental facility (T - temperature indicator; P - pressure indicator).

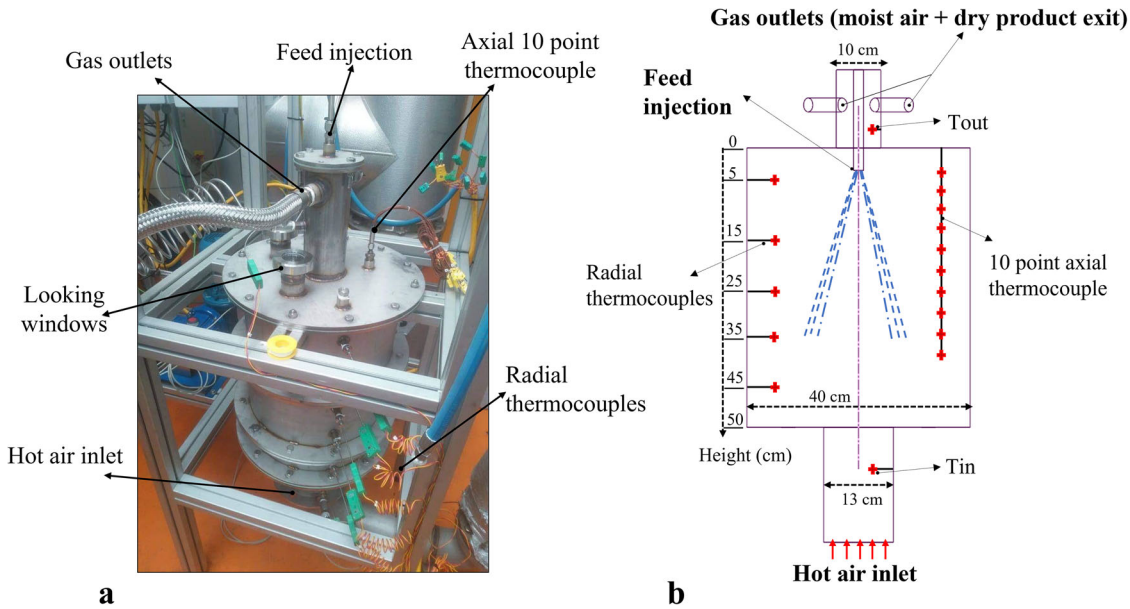

Figure 3. The counter-current spray dryer (a) and its schematic representation (b) (+ signs indicate thermocouple positions).

thermocouples inside the dryer is presented in Figure 3. Five thermocouples are mounted radially into the chamber, while a single thermocouple with ten measuring points is mounted axially from the top of the chamber, on the opposite side to the radial probes. This is done to assess the symmetry of the processes that occur inside the reactor and to provide data from variable positions. Additionally, two thermocouples are located in the center of the chamber: in the hot air inlet cylinder (Tin) and the exhaust chimney (Tout). They indicate the inlet and outlet temperature in the dryer and the possibility of the droplets penetrating into the hot air inlet cylinder or the exhaust chimney. Furthermore, the temperature is measured at the outlet of the cyclone (Texh). The atomization pressure was recorded at the pump outlet using a digital pressure transducer (accuracy $\leq$ 0.5%). All data acquisition was performed via NI myDAQ (National Instruments) combined with the LabVIEW interface.

A total of 16 experiments were performed. The tests were done under different conditions with respect to inlet air temperature ($260-360\,^{\circ}C$), air mass flow rate (300- 481 kg/h), feed flow rate (17-28 kg/h), and mean droplet sizes, as shown in Table 2. Finally, based on the outcome of the studies with

Table 2. Overview of the process conditions for the experimental tests, W-water, SM- skim milk.

Exp #	Feed	Nozzle orifice (mm)	T_{in} (°C)	T_{out} (°C)	T_{exh} (°C)	Airflow (kg/h)	Feed flow (kg/h)	Feed pressure (bar)	**Droplet SMD (μm)**
1	W	0.5	266 ± 2	105 ± 5	112 ± 1	481	21	55 ± 1	40
2	W	0.5	307 ± 2	140 ± 3	132 ± 1	481	21	55 ± 1	40
3	W	0.5	359 ± 4	185 ± 5	163 ± 4	481	21	55 ± 1	40
4	W	0.5	360 ± 2	187 ± 3	164 ± 2	481	21	55 ± 1	40
5	W	0.5	360 ± 1	184 ± 3	163 ± 2	386	21	55 ± 1	40
6	W	0.5	360 ± 1	166 ± 3	147 ± 3	300	21	55 ± 1	40
7	W	0.5	361 ± 1	188 ± 2	186 ± 3	481	17	36 ± 1	49
8	W	0.5	361 ± 1	186 ± 5	176 ± 1	481	19	45 ± 1	44
9	W	0.5	361 ± 1	186 ± 2	165 ± 1	481	21	55 ± 1	40
10	W	0.5	361 ± 1	184 ± 2	162 ± 1	481	23	60 ± 1	37
11	W	0.6	353 ± 1	179 ± 1	157 ± 1	386	23	31 ± 1	60
12	W	0.6	352 ± 2	174 ± 2	149 ± 1	386	25	36 ± 1	56
13	W	0.6	349 ± 1	167 ± 1	143 ± 1	386	27	41 ± 1	51
14	W	0.6	343 ± 2	161 ± 2	138 ± 1	386	28	47 ± 1	44
15	SM	0.5	253 ± 5	140 ± 2	119 ± 1	481	18	36 ± 4	48
16	SM	0.6	237 ± 3	132 ± 1	117 ± 1	481	21	25 ± 1	77

water as a feed, additional conditions were selected for skim milk tests. Each experiment was run for sufficient time to allow a steady-state operation, typically 5-15 minutes. The skim milk tests began from spraying water, and once the desired stable steady-state condition was reached, water feed was shifted into the skim milk.

After the skim milk tests, samples obtained from the cyclone were analyzed for their powder properties. The Particle Size Distribution (PSD) of the skim milk powder was evaluated using a multiwavelength laser diffraction particle size analyzer (Beckman Coulter LS 13320 CAMSIZER®) in compliance with ISO 13320:2020. The samples were characterized by the Dv90, Dv50, and D_{32}, quantities of volumetric distributions. In addition to PSD, an Environmental Scanning Electron Microscope Philips/FEI XL30 (ESEM) at 10-20 kV was employed to examine the surface structure and morphology of the obtained skim milk powder samples. Lastly, the particle moisture content of the samples was determined using a thermogravimetric moisture analyzer (Satorius® MA100) in accordance with ISO 5071:1996.

For the experiments, a commercial skim milk powder as provided by FrieslandCampina, the Netherlands, was used. Before the experiments, 20 wt.% of skim milk powder was reconstituted to fresh water at room temperature (20 °C). The milk concentrate mixture was stirred for a period of 5–10 minutes until a homogenous mixture was attained.

3. Droplet size distribution results

The droplet size measurements are taken in the near field of the primary breakup location (primary atomization), i.e., at the point at which the liquid sheet breaks up into ligaments and disintegrates into droplets.[65] At viscosity of 1 mPa.s and 5 mPa.s, the distance of primary break up was found to be approximately 2 cm from the nozzle tip, while the distance increased to 4 cm for 30 mPa.s. The atomization performance and spray characteristics are investigated for three different nozzle orifice diameters and three different viscosities, as shown in Tables 1 and 3.

The performance of the atomization is characterized using the Sauter Mean Diameter (SMD or D_{32}) to compare the droplet size distributions at different conditions. The SMD gives the mean droplet size in the spray, and it is a relevant measure when the surface mass transfer and evaporation processes are important.[52] Its definition is given by Eq.(2) where D_{drop} is the effective droplet diameter based on its area.

$$SMD = \frac{\sum D_{drop}^3}{\sum D_{drop}^2} \quad [2]$$

Additionally, the Dv10, Dv50, and Dv90 volume diameters were also calculated. These represent, respectively, the equivalent droplet diameters for which 10, 50, and 90% of the total volume spray is made; see also Table 3 for details. Since, in general, the trend presented by different droplets as a function of viscosity and atomizer's orifice size is similar, only the SMD is discussed further in detail.

Figures 4 and 5 give the SMD and droplet distribution as a function of atomization pressure for three different viscosities and three different orifice diameters. With the increase in liquid pressure for any given nozzle orifice diameter, the SMD decreased almost linearly. For instance, increasing the liquid pressure from 10 to 30 bar for nozzle 1 resulted in a decrease of the SMD from 61 μm to 51 μm. Similarly, for nozzle 2 and nozzle 3, the SMD decreased from 79 to 60 μm and from 86 to 66 μm, respectively. The smallest droplet diameters were observed for nozzle 1 with

Table 3. Droplet size distribution and particle velocities for different nozzle orifices and viscosities at atomization pressure of 30 bar, Vp- Particle average velocity.

	Dv10 (μm)			Dv90 (μm)			Dv50 (μm)			D_{32} (μm)			V_p (m/s)		
Viscosity (mPa-s)	1	5	30	1	5	30	1	5	30	1	5	30	1	5	30
Nozzle 1 (0.5 mm)	32	32	53	100	106	285	60	64	130	52	54	100	43	36	44
Nozzle 2 (0.6 mm)	35	42	48	134	162	638	73	87	152	61	73	104	48	44	30
Nozzle 3 (0.7 mm)	38	45	58	149	189	471	79	97	145	66	79	112	47	46	38

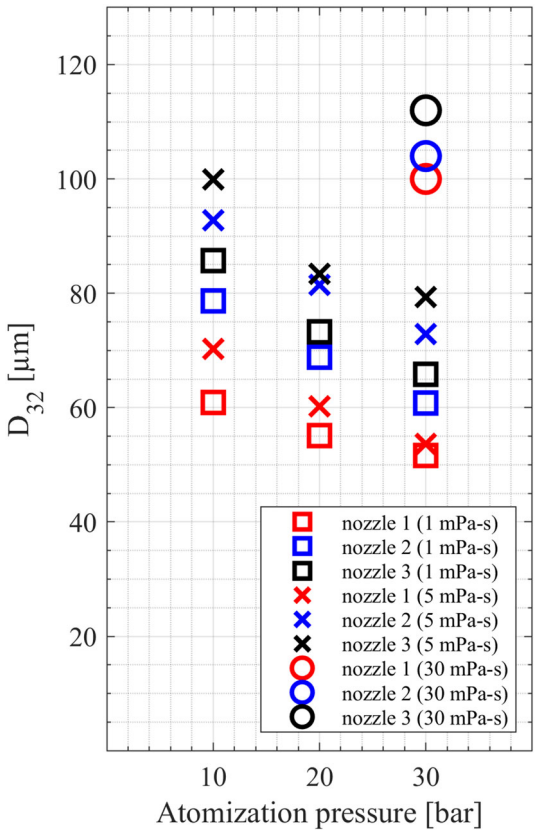

Figure 4. SMD as a function of liquid pressure and viscosity for different orifice diameter nozzles.

an orifice diameter of 0.5 mm, while the largest orifice diameter of 0.7 mm produced the biggest droplets (see Table 3). This is due to the fact that an increase in spray pressure enhances the kinetic energy of the feed, leading to a reduction of the liquid sheet stability, and in consequence, to the generation of smaller droplets. In contrast to the effect of atomization pressure, an increase in liquid viscosity from 1 mPa.s (0 wt.% TS) to 5 mPa.s (20 wt.% TS) resulted in a bigger SMD. The difference in droplet diameters (for two viscosities) is larger at lower atomization pressures and bigger orifice diameters, see Table 3. Furthermore, it is worth noticing that the SMD for 0.5 mm nozzle at the viscosity of 5 mPa.s is smaller than the SMDs generated by 0.6 mm and 0.7 mm nozzles at 1 mPa.s. This shows the influence of the atomizer on the spray properties.

A further increase of liquid viscosity to 30 mPa.s (40 wt.% TS) delays the spray break up and results in an increase of the droplet's diameter. This is since the kinetic energy needed to disintegrate the liquid sheet must increase as well in order to overcome the internal forces in the feed film.[52,53,57,65,66] The influence of the viscosity on droplet diameters is also illustrated in the spray images, see Figure 6. Here an excessive formation of the ligaments and big droplets is visible for 30 mPa.s viscosity spray. The difference is less apparent between lower viscosities.

Figure 7 shows the effect of atomization pressure and viscosity on the average velocity of the droplets for the three investigated nozzles. Evidently, the droplet velocity increases for enhanced atomization pressure while decreases with an increase in liquid viscosity. A deviation from this pattern, however, is observed for nozzle 1 at the viscosity of 30 mPa.s. In this case, the droplet velocity goes from 42 m/s at 5 mPa.s to 44 m/s at 30 mPa.s. This deviation could be attributed to the difference in the liquid sheet breakup in comparison to other investigated cases. Furthermore, the higher velocities of the droplets produced for the nozzles with bigger orifice diameters (at a fixed pressure) can be attributed to the increased volumetric flow rates in these nozzles. Initially, the velocity of the liquid is at its maximum at the orifice tip, and then due to the hydrodynamic and aerodynamics instabilities, the liquid sheet breaks up into ligaments and droplets. The droplets are deaccelerated under the influence of drag forces. Typically, the smallest droplets are affected the most, while the velocity of the big droplets near the orifice stays almost unchanged. This behavior is related to the low momentum of the small droplets and drag forces which slow them down quickly after leaving the nozzle orifice. Furthermore, Figure 8 shows that the small droplets of the same size, due to different trajectories/locations in the spray, may have different velocities. As the droplet size increases, droplets tend to attain a homogeneous velocity in the range of 40-60 m/s.

The implication of different droplet sizes and velocities (shown in Figure 8) is crucial in a spray drying

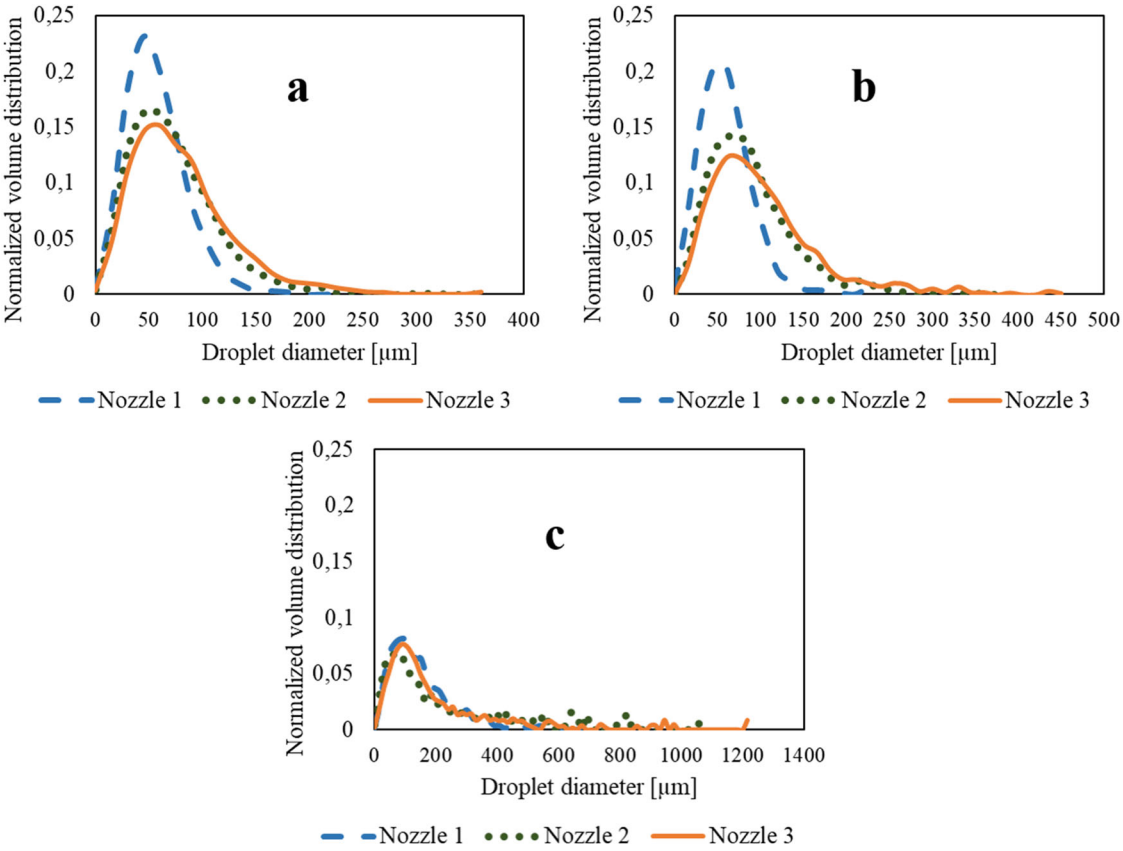

Figure 5. Initial droplet size distribution for the viscosity of 1 mPa.s (a), 5 mPa.s (b), and 30 mPa.s (c) for the different nozzle orifice diameters, at an atomization pressure of 30 bar.

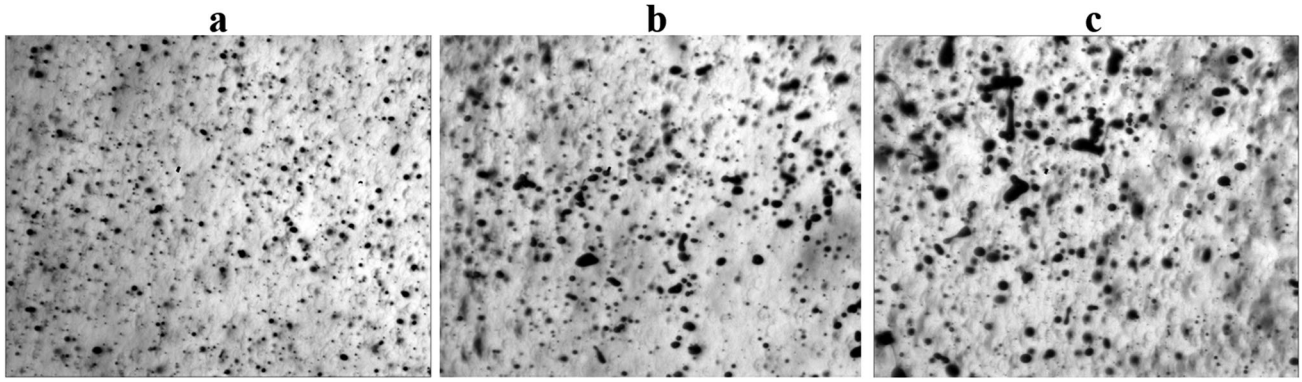

Figure 6. Example droplet images from nozzle 1 for 1 mPa.s (a) 5 mPa.s (b) and 30 mPa.s (c), at an atomization pressure of 30 bar. (Image "a" and "b" are taken at 2 cm while image "c" is taken at 4 cm from the nozzle tip).

process, since for the same airflow conditions, different droplets may have different trajectories in the reactor, and thus, different drying history. A small droplet can evaporate quickly, whereas the big one would require a longer time to evaporate. Similarly, the momentum of small particles is the least and would be most affected by the counter flow air. In contrast, the big particles with maximum inertia can penetrate far in the reactor leading to product deposition on the walls.

4. Counter flow spray drying experiments

The experimental setup allowed us to investigate the effect of various process parameters, i.e., air inlet temperature, air mass flow rate, feed flow rate, and SMD of the spray on the temperature profiles in the dryer for water tests, and the influence of droplet size on deposition and powder characteristics for the skim milk tests. A total of 16 spray drying experiments were performed, including 14 water tests and 2 skim

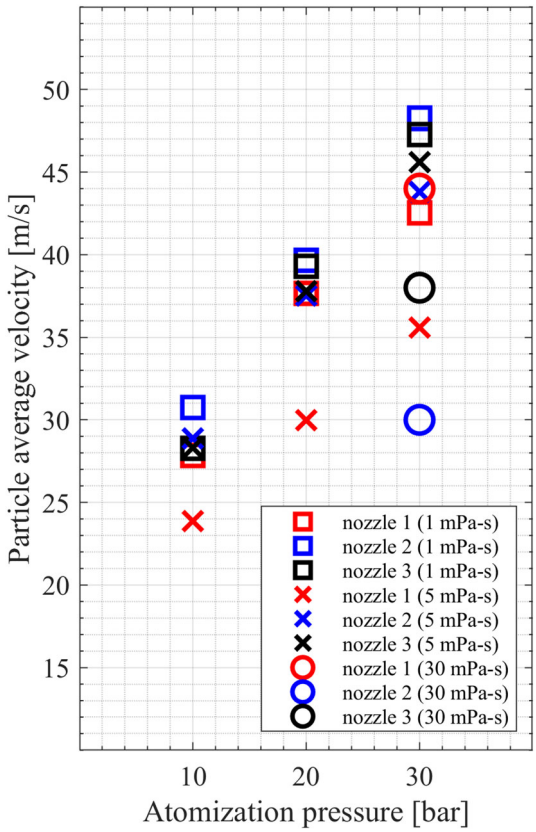

Figure 7. Particle average droplet velocity as a function of liquid pressure and viscosity for different orifice diameter nozzles.

milk tests to evaluate the performance of a counter-current spray drying mechanism. A complete list of experimental conditions is presented in Table 2. It shows the influence of investigated conditions on the inlet, outlet, and exhaust air temperature.

During the dry run tests (without water spray), considerable heat losses with an approximate temperature difference of 50–60 °C were noted between the dryer inlet and outlet locations. However, the heat losses to the environment reduced as soon as the feed was initiated due to the smaller thermal gradients. Still, the heat losses could affect the final air temperatures by approximately 25–30 °C.

4.1. Water spray experiments

The initial parametric studies (air inlet temperature and air mass flow rate) are conducted using nozzle 1 (0.5 mm) due to the superior atomization behavior and narrow droplet size distribution. Next to that, for an assessment of the effect of the droplet size, also nozzle 2 (0.6 mm) is used. The results from the water spray experiments define the conditions for the skim milk tests.

4.1.1. Influence of air inlet temperature

The drying air temperature is one the most important parameters for the drying process since it dictates the initial temperature difference between the air and droplets, and thereby the evaporation rate of droplets. For the same feed rate of 21 kg/h and mean droplet size of 40 µm, experiments are conducted for three different air inlet temperatures: 266 °C, 307 °C, and 359 °C (see Table 2). As the air inlet temperature is increased, the temperature in the chamber also rises. This is shown in Figure 9, depicting temperature profiles in the chamber at different axial heights. The temperature pattern in the chamber suggests a central hot core flow that enters via the bottom of the reactor and flows straight upwards while expanding radially outwards to the walls. The air temperatures are the highest in the top part, with a gradual decrease toward the bottom of the chamber (as seen in Figure 9b). Such a profile indicates recirculation of air due to sudden expansion of the hot air jet, which leads to the formation of low velocity or dead zones along the bottom wall of the dryer. Furthermore, the air temperature measured by the axial multipoint thermocouple, in general, is slightly higher in comparison to the radial thermocouples. This reveals slight asymmetry in the flow with hot air deflecting more toward the axial multipoint thermocouple. During the tests without water spray, the asymmetry is not so pronounced, suggesting that this is a consequence of the interaction between the counter flow hot air and feed spray.

For the same mean droplet size, increasing the air inlet temperature should give faster evaporation rates due to the bigger temperature difference between the air and droplets.[67] The influence of the lower air inlet temperature on the evaporation rate is evident via Figure 9a. In Experiment 1 (inlet air temperature 266 °C), all three temperature probes placed in the reactor at 25–45 cm from the top, measured only the wet-bulb temperature of air (approximately 60 °C), suggesting constant impingement of water droplets on the thermocouple surfaces. Increasing the air inlet temperature to 307 °C (Experiment 2) resulted in an overall increase of air temperature in the dryer; however, at locations 25 and 35 cm, the thermocouple probes still recorded low air temperatures of around 60–70 °C (see Figure 9a), suggesting that wetting of probes still takes place. In Experiment 3, the air temperature in the bottom part of the chamber was significantly higher, approximately about 130–150 °C compared to 60 °C in Experiment 1 and 80–100 °C in Experiment 2, see Figure 9a and b.

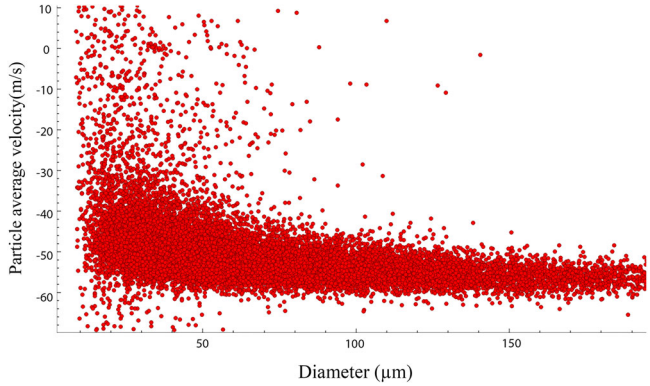

Figure 8. Droplet velocities as a function of droplet diameters (atomization pressure of 30 bar and liquid viscosity of 30 mPa.s for nozzle 1).

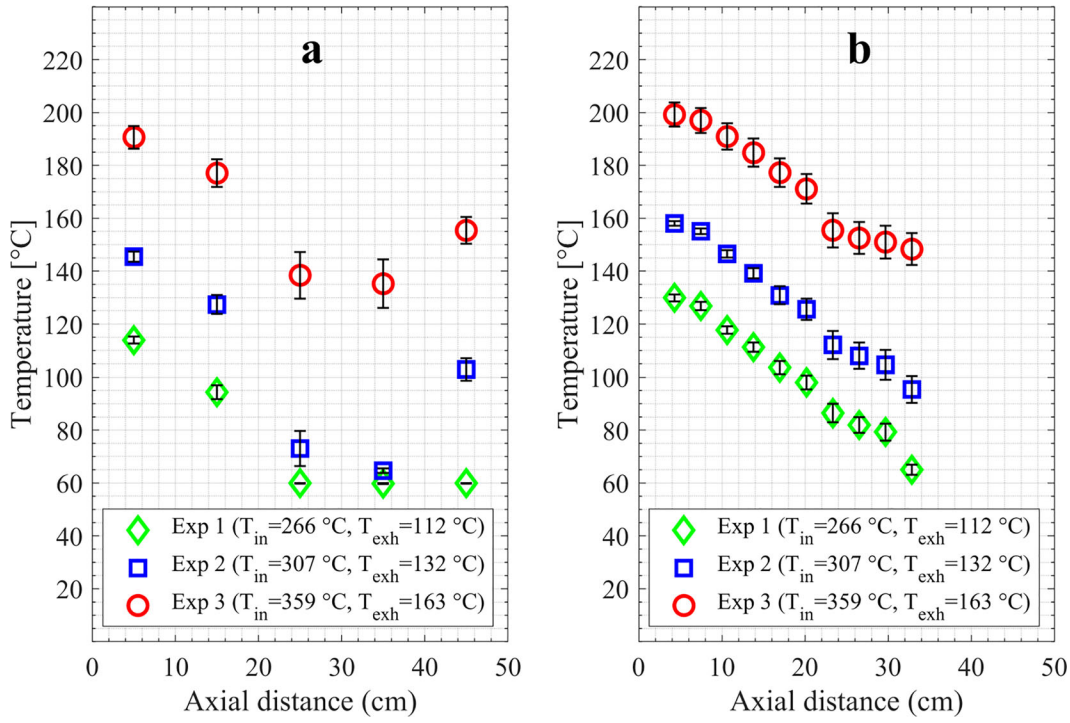

Figure 9. Temperature profiles along the dryer length (0 cm is at the top of the dryer) for radial thermocouples (a) and axial multi-point thermocouple (b), at different air inlet temperature; (air mass flow rate 481 kg/h, feed rate 21 kg/h, droplet SMD 40 μm).

4.1.2. Influence of airflow rate

To investigate the effect of the airflow rate on the drying performance of the reactor, the air inlet temperature, feed flow rate, and droplet size is kept fixed, whereas the air inflow is varied between 300 – 481 kg/h, see Table 2. For the airflow rate of 481 and 386 kg/h (Experiment 4 and Experiment 5), the temperature profiles in the dryer were almost the same; only minor differences (about 5–10 °C) were observed, see Figure 10. The lowest air temperature was observed for the airflow rate of 300 kg/h. Lowering the air mass flow rate from 481 to 300 kg/h (at a constant temperature) decreased the air velocity and total energy input to the dryer by 40%. These have led to an increase in the penetration depth of droplets as a consequence of drag reduction and extension of the evaporation process. This can be further observed in Figure 10a, where the air temperature is approximately 20–60 °C lower compared to the experiments performed at higher flow rates (386 and 481 kg/h). This effect is especially pronounced in the middle part of the chamber, where the spray may impact thermocouples (as discussed in Section 4.1.1).

A similar trend can be observed at the axial multi-point thermocouple (Figure 10b), where the air temperatures are the highest in the top part of the reactor and lowest in the bottom part of the dryer. The temperature differences between all three experiments are much

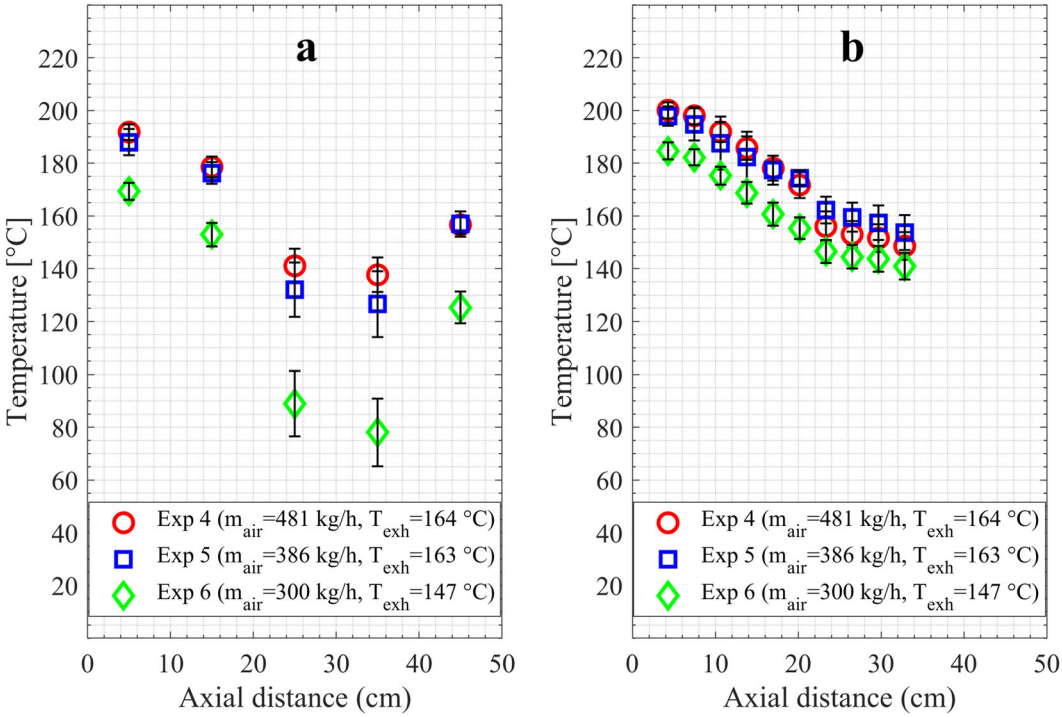

Figure 10. Temperature profiles along the dryer length (0 cm is at the top of the dryer) for radial thermocouples (a) and axial multipoint thermocouple (b), at different air mass flowrate; (air inlet temperature ≈360 °C, feed rate 21 kg/h, droplet SMD 40 μm).

smaller, approximately 5–10 °C. For the lowest airflow rate, i.e., 300 kg/h, the temperature at the air outlet and exhaust pipe was equal to 166 °C and 147 °C, respectively. The tests with a higher airflow rate of 481 and 386 kg/h had nearly the same outlet and exhaust temperature of approximately 184 °C and 164 °C, respectively. Since the air inlet temperature and feed rate are kept the same for these experiments, the difference of 20 °C is associated with the lower amount of net energy supplied to the dryer. Again, some differences between the temperature measurement probs (axial and radial) were observed, suggesting asymmetry in the flow pattern.

4.1.3. Influence of the feed rate

The influence of the feed rate and atomization quality is investigated in this section for nozzle 1 and nozzle 2. For pressure nozzles, as used in this study, the feed rate is proportional to the atomization pressure. Thus, by spraying higher feed rates, the atomization pressure is increased, leading to enhanced droplets' injection velocity and smaller SMD. Additionally, for the same air inlet temperature and air mass flow rate, increasing the feed rate results in a bigger temperature drop as a consequence of a higher evaporation rate. Furthermore, by increasing the feed rate, the number density of droplets is expanded, thereby providing a larger surface area for the heat and mass exchange of droplets with air.

Figure 11 shows that the temperature profiles and maximum evaporation zones in the dryer are correlated to the atomization parameters, namely: feed rate, droplet diameter, and velocity.

The maximum evaporation zone and lowest air temperatures are in the top part of the dryer for a feed rate of 17 kg/h and shifts lower to the location of about 15–35 cm when the feed rate is increased (Figure 11a and b). The variations in the temperature profiles arise mainly due to the atomization characteristics and the interaction of spray with the counter-flow hot air. In the case of the lowest feed rate, the injection velocity is relatively small, leading to quick deacceleration caused by the drag forces of the counter-flowing air. Since the feed rate is small, the majority of the evaporation happens close to the atomizer, i.e., in the top part of the dryer (0–10 cm), resulting in higher air temperatures downstream of the dryer (>15 cm from top). Increasing the feed rate to 19 kg/h (and further) forces the droplets to penetrate further in the dryer, shifting the maximum evaporation zones toward the middle (15–20 cm) or bottom part of the dryer (>20 cm), see also Figure 11b.

For the feed rate of 23 kg/h, the atomization pressure becomes 60 bar, while the injection velocity is approximately equal to 110 m/s. These conditions cause droplets to move very quickly to the walls before they are fully evaporated. The big droplets that do not evaporate impinge then the middle/bottom part of the dryer and

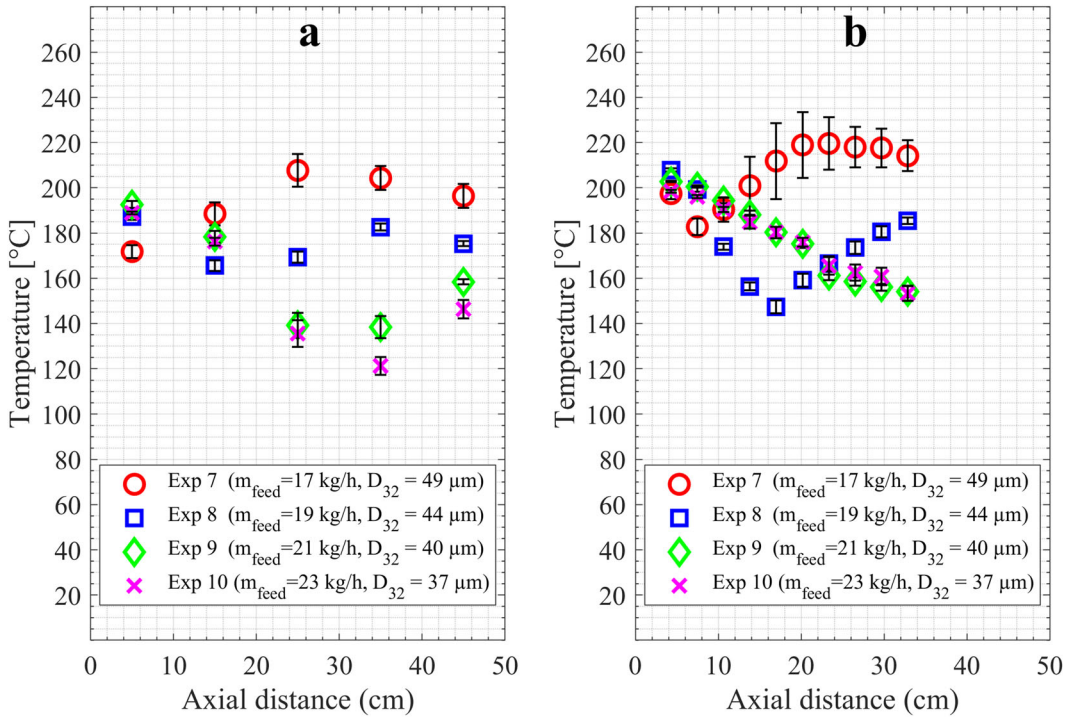

Figure 11. Temperature profiles along the dryer length (0 cm is at the top of the dryer) for radial thermocouples (a) and axial multipoint thermocouple (b) at different spray feed rates and droplet size for nozzle 1; (air inlet temperature ≈360 °C, air mass flow rate 481 kg/h).

accumulate at the bottom wall (seen via video recordings). This is also evident from the exhaust air temperatures where an increase of the feed rate from 21 to 23 kg/h only resulted in the temperature decrease by 3 °C. For both cases, the maximum evaporation zone takes place in the middle-bottom part of the dryer. This shows that even though the droplet size decreases to approximately 37 µm (see Experiment 10), the evaporation does not necessarily increase due to the very high injection velocity of the droplets, small residence time, and impingement to the walls.

Similar trends are observed at the radial thermocouple for all feed rates. Figure 11a illustrates the lowest air temperature (130 °C) in the bottom part of the chamber (between 35 and 45 cm) for the highest feed rates of 21–23 kg/h, while in the top part of the dryer (0–20 cm) the lowest air temperature (160–180 °C) is recorded for the small (17–19 kg/h) feed rates.

Figure 12 shows the influence of feed rate and droplet size on the temperature profiles in the dryer for nozzle 2 (orifice diameter of 0.6 mm). The bigger orifice diameter of 0.6 mm results in a higher liquid flow rate at a lower atomization pressure producing relatively bigger droplet sizes compared to nozzle 1. For all investigated feed rates, the temperature profiles follow the same pattern. The highest air temperature is observed in the top part of the chamber (0–15 cm), with a gradual decrease of air temperature along the chamber height. The biggest temperature drop, and subsequently, the maximum evaporation, occurs in the middle-bottom region of the dryer between 20 and 45 cm. Furthermore, Figure 12b shows that as the feed rate is increased (up to 28 kg/h), the air temperatures decrease in the middle part of the chamber (compared to lower feed rates), depicting the influence of droplet size on the evaporation process. In general, the behavior of the experiments with nozzle 2 resembles the experiments with the highest flow rates for nozzle 1. In general, the increase in feed rate showed similar behavior to reducing air flow rate or air inlet temperature, where evaporation continues downstream in the chamber due to smaller droplet evaporation rates along the dryer length. Similar observations for spray drying of whole milk in a counter-current configuration dryer were reported by Razmi et al.[15] using a 1d modeling approach.

4.2. Skim milk experiments

To perform skim milk drying tests, we selected conditions from the water experiments where the outlet temperature is roughly below the glass transition temperature of skim milk powder. This was approximately 20–30 °C above the glass transition temperature of pure lactose (101 °C).[68] Here, only Experiment 1 with an air inlet temperature of 266 °C resulted in an

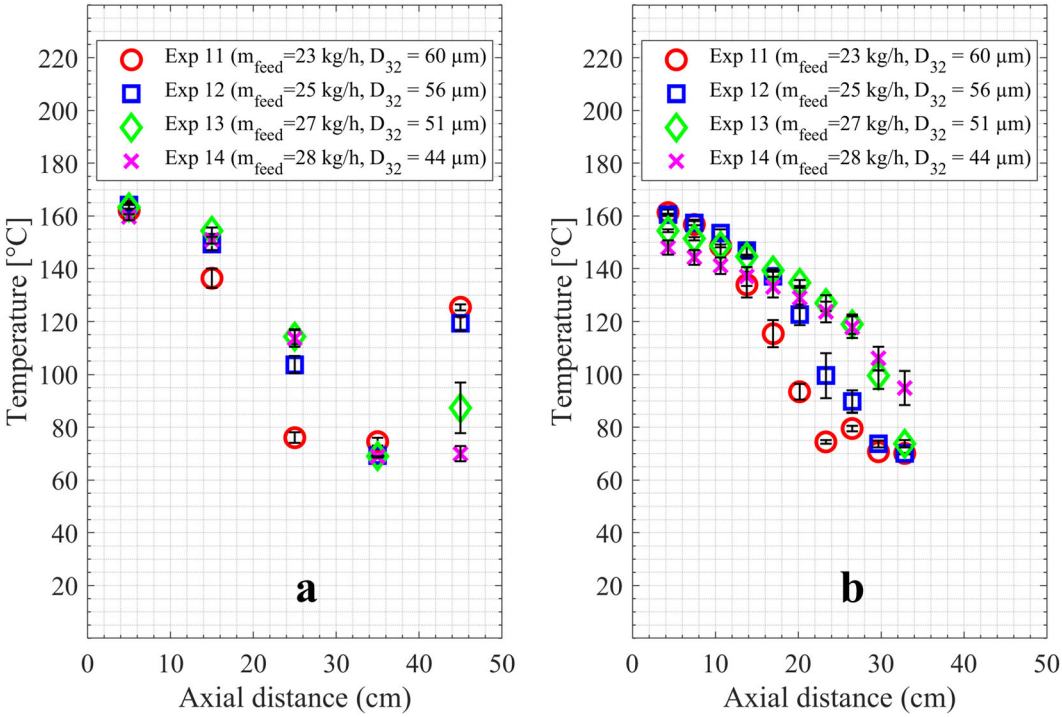

Figure 12. Temperature profiles along the dryer length (0 cm is at the top of the dryer) for radial thermocouples (a) and axial multipoint thermocouple (b) at different spray feed rates and droplet size for nozzle 2; (air inlet temperature ≈360 °C, air mass flow rate 386 kg/h).

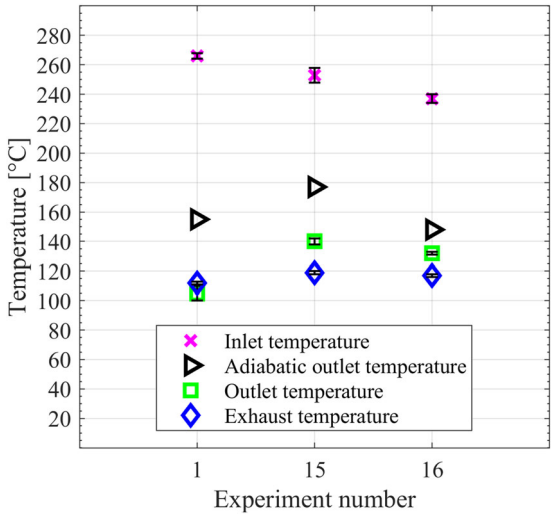

Figure 13. Temperature data for the Experiments: 1, 15, and 16; (air inlet temperature ≈260 °C, air mass flow rate 481 kg/hr, feed rate ≈21 kg/h).

outlet temperature of 105 °C; however, some thermocouples wetting by impinging of droplets was observed. It is expected that this behavior may not be present in the experiments with skim milk since actually less water must be evaporated for the same feed flow.

4.2.1. Effect of the nozzle parameters on the temperature profiles

For skim milk experiments, both nozzles, i.e., with an orifice diameter of 0.5 and 0.6 mm, were selected. It should be noted that for Experiment 15, with the orifice diameter of 0.5 mm, it was not possible to maintain the atomization pressure at 52 bar. This is due to the higher viscosity of the skim milk in comparison to the water tests, see Tables 1 and 2. Therefore, in this experiment, an atomization pressure of 36 bar was used, resulting in a slightly lower feed rate of approximately 18 kg/h instead of 21 kg/h.

Figure 13 shows the inlet, outlet, exhaust, and adiabatic outlet temperature obtained for the selected experiments. The adiabatic outlet temperature is calculated based on Equation 3, where the heat of vaporization of water (H_v) and heat capacity (C_p) of air is taken as 2453 kJ/kg.K and 1.035 kJ/kg.K, respectively. Taking into account that the actual temperature in the reactor is about 30-40 °C lower due to heat losses, the estimated exhaust temperature corresponds well to the experimental data.

$$T_{adiabatic\ \ outlet\ \ temperature} = T_{in} - \frac{\left(\left(m_f * (1 - x_{solids}) * H_v\right)\right)}{m_{air} * \ C_p} \quad [3]$$

where m_f is the feed rate, x_{solids} is the solids concentration in the feed (20 wt.%), and m_{air} is the mass flow rate of air.

Although the gas outlet temperature for both experiments with skim milk is similar, the temperature profiles inside the reactor, due to different spray

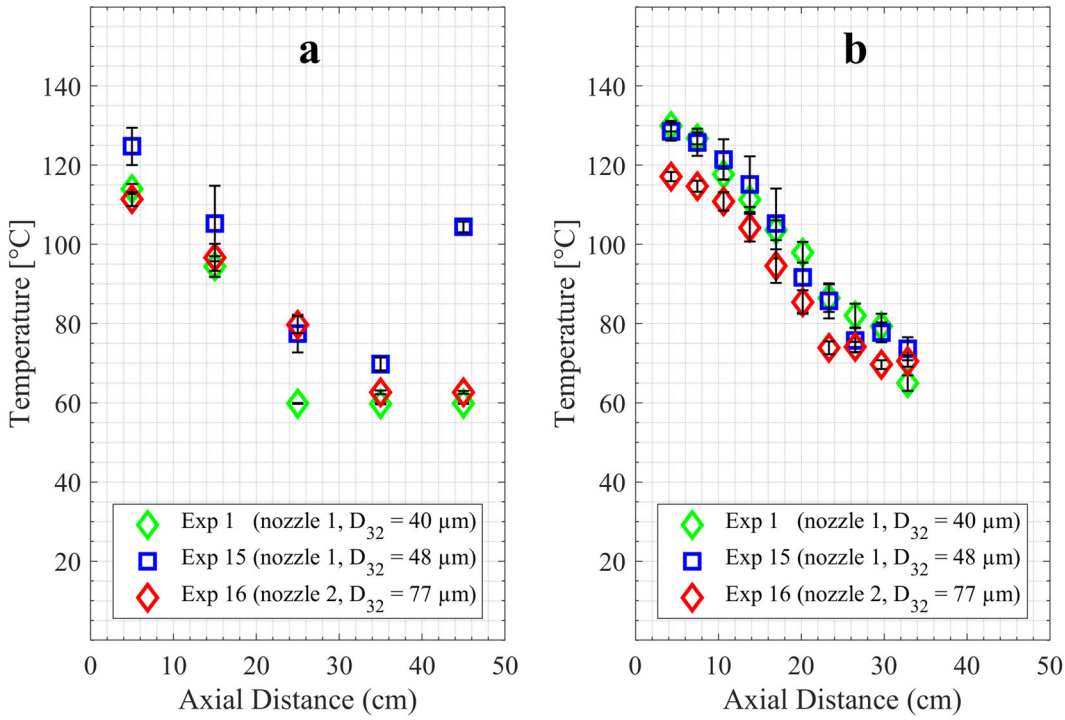

Figure 14. Temperature data for the Experiments: 1, 15, and 16 along the dryer length (0 cm is at the top of the dryer) for radial thermocouples (a) and axial multipoint thermocouple (b); (air inlet temperature ≈260 °C, air mass flow rate 481 kg/hr, feed rate ≈21 kg/h).

parameters, can differ. As can be seen from Figure 14, close to the nozzle and in the middle part of the reactor, there is no significant difference in the results of the experiment with nozzle 1 and nozzle 2. Only downstream of the reactor (>25 cm from the top), it is possible to note that for nozzle 2, all probes (between 25 and 45 cm) measure the wet-bulb temperature of the air, whereas, for nozzle 1, the air temperatures are relatively high suggesting minimal wetting of the probes and thus better drying characteristics of spray with smaller SMD. Comparing the data with Experiment 1 (water feed), the air temperature from the skim milk feed experiments is slightly higher due to the smaller amount of water that has to be evaporated in the reactor. The effect of the spray parameters on the evaporation process is similar as discussed in section 4.1; thus, the discussion here is not repeated.

4.2.2. Influence of skim milk droplet size on deposition in the dryer

The influence of initial droplet size on milk sticking and deposition in the dryer is evaluated qualitatively after each of the investigated cases. The deposition pattern, in general, reflects the temperature profiles in the dryer. The temperature of the air is the highest in the top part and gradually decreases along the dryer length with the lowest air temperatures at its bottom (33–50 cm). The maximum deposition of milk particles occurs along the top wall (0–15 cm), while almost little to no deposition in the middle part of the dryer (20–33 cm), as presented in Figure 15 for both nozzles. Furthermore, the milk droplets that are not completely dried accumulate as a liquid or semi-dried particles on the bottom wall surface or enter the inspection windows (marked in red in Figure 15a).

Looking closely at the deposition patterns, it could be noted that for the initial droplets' SMD equal to 77 µm (nozzle 2), actually only a thin layer of deposition is visible at location 0-10 cm from the top plate. In contrast, quite pronounced deposition is observed for droplets with SMD of 48 µm (nozzle 1). This can be further observed in Figure 15c, where a thick layer of dried powder is deposited on the top walls for nozzle 1. In this case, all particles that impact the top wall are completely dry and, after deposition, got sintered and scorched. These particles are dry and could be scraped off by hand (as visible by the scratch marks in Figure 15a). In comparison, when a bigger droplet size of 77 µm was employed, the particles appeared to be semi-dry at the moment of their impact to the walls (see also the sliding deposition pattern in Figure 15b and d). In this scenario, only a small layer of fine particles was deposited in the top part (0–10 cm) of the dryer (Figure 15d). In both studies, the extremely fine particles were instantly

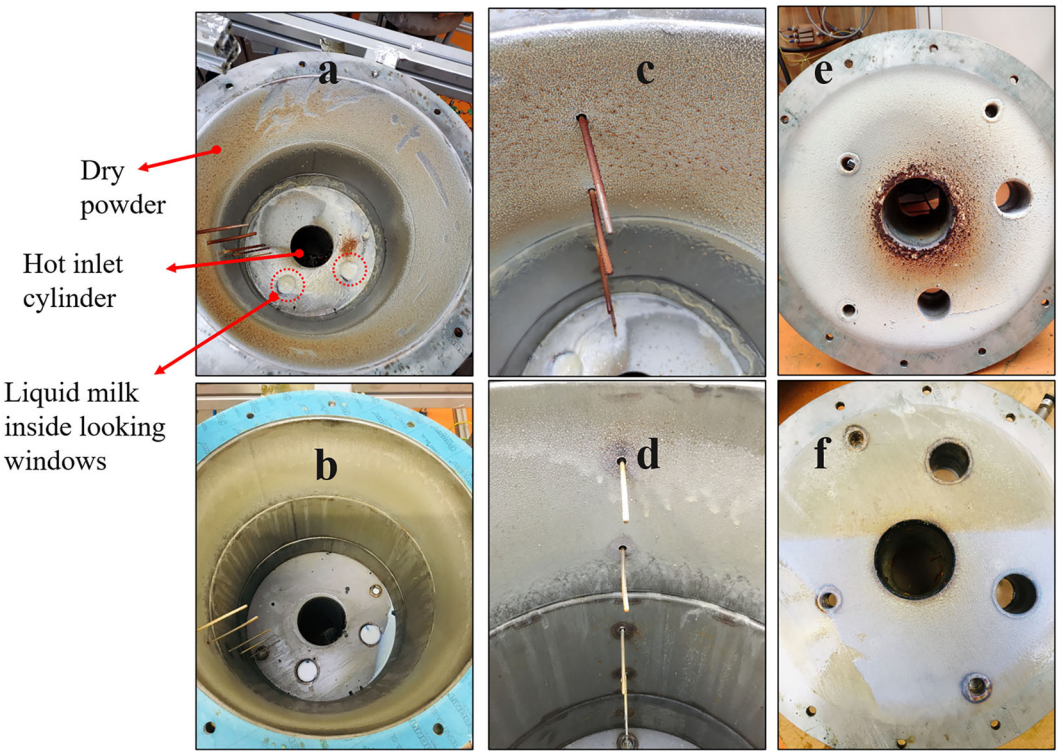

Figure 15. Deposition pattern in the dryer: (top) results for nozzle 1, (bottom) results for nozzle 2, (left) top-down view from the inside of the dryer, (middle) zoom of the top section with thermocouples, (right) top wall of the dryer with visible viewpoints and exhaust chimney.

Table 4. Powder particle size distribution and moisture content.

Nozzle	Dv90 (μm)	Dv50 (μm)	D_{32} (μm)	Moisture content (wt.%)
Nozzle 1	292	29	21	6.88
Nozzle 2	102	25	19	7.04
Ref.	150	74	56	4.01

deflected back toward the top wall of the reactor (Figure 15e and f), causing deposition there. The sticking in the top part of the dryer occurs mainly due to the coupled effect of air temperature being higher than the glass transition temperature of skim milk droplets[69] and fast-drying of smaller size particles. The burn-out of milk deposits around the gas outlet chimney appeared from the shutdown procedure when the feed pump was turned off, and still, high air temperature flows in the reactor were visible. This was confirmed by the video recordings.

O'Donoghue et al.[70] determined the stickiness curves for different particle sizes of skim milk powder using a simple fluidization technique. The results showed that fine particles, due to their bigger surface area, promote the formation of liquid bridges causing adhesion or cohesion phenomena. Walmsley et al.[69] demonstrated that as the particle size is decreased, their glass transition temperature reduces significantly, making the particles more susceptible to deposition and sticking. The experimental outcome aligns well with the above-presented literature findings.

In contrast to the smaller particles, larger-sized particles penetrate deeper in the dryer and have slower drying rates which makes them sticky due to their higher moisture content. As a consequence, these semi-dry particles, after impacting the mid/bottom section of the dryer, create deposition which looks more like a film of skim milk (see Figure 15b and d). The reason for such a deposition pattern could be attributed to the effects of feed condensation on the cold bottom walls of the dryer, as discussed by Ozmen and Langrish.[43] Here, due to the combined effect of low-velocity zones present near the bottom surface of the dryer and the continuous evaporation of the accumulated liquid film on the bottom wall, the air temperature there is relatively low. This ultimately results in a greater deposition rate due to the droplets or semi-dried milk particles falling directly or sliding from the walls into the liquid film that turns into a rubbery deposition pattern. Such deposition (semi-liquid or rubbery) occurring in the conical bottom section of a co-current dryer were also identified by other researchers.[44,71] For spray drying of skim milk in a counter-current configuration, our findings of two sticky zones at the top and bottom of the dryer, due to different penetration depths of droplets/

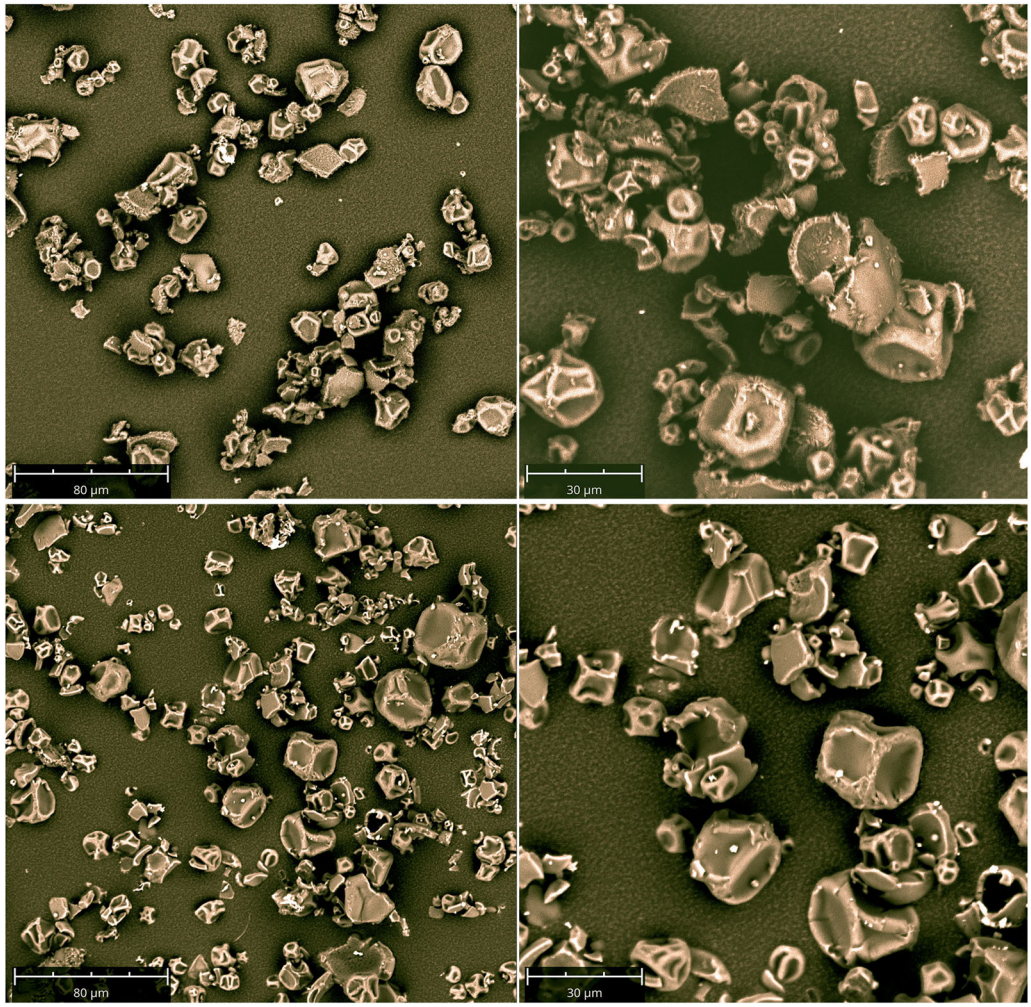

Figure 16. SEM images of recovered powder samples at different magnifications, top row: nozzle 1, bottom row: nozzle 2.

particles, are well supported from the numerical study of Jubaer et al.[14]

4.2.3. Powder characteristics

To identify the particle sizes that deposit on the dryer walls and leave with the outflowing gas, we investigated the final Particle Size Distribution (PSD) of the samples recovered in the cyclone separator. The Dv90, Dv50, and D_{32} particle sizes of the obtained powder, along with the final moisture content, are shown in Table 4. From the table, it is visible that the Dv90 particle size for nozzle 1 is much bigger. This again points to the fact that small particles, due to their relatively bigger surface area and low glass transition temperature, are more prone to sticking to each other and form agglomerates.[69]

Even though the initial droplet SMD produced by both nozzles is different, namely 48 µm for nozzle 1 and 77 µm for nozzle 2, the SMD of the recovered product is very alike, i.e., 21 µm for nozzle 1 and 19 µm for nozzle 2. Also, the moisture content of the recovered particles is similar, i.e., 6.88 wt.% for nozzle 1 and 7.04 wt.% for nozzle 2. The similar final particle sizes recovered under different atomizing conditions (SMD, droplet velocity) indicate that the particles leaving with the outflowing gas depend largely on the airflow conditions (inlet velocity) in the dryer since these were kept constant. Furthermore, this also indicates an optimum droplet size that can be dried successfully without the risk of particles sticking to the dryer walls, as observed from the lack of particle deposition pattern on the bottom part of the dryer walls (beyond 20-30 cm). The distribution of particle sizes leaving the dryer or depositing on the walls suggests that additional secondary swirling flows with high centrifugal forces must be applied for efficient air-particle separation.

Additionally, the PSD of the samples is compared to the reference powder obtained from the company. It is seen that the reference product has a much bigger particle diameter; this is because the reference powder was produced in the conventional co-current

spray dryer where the droplets spend significant time in the reactor before being completely dried out and evacuated to fluidized beds, where post agglomeration takes place. In addition, nozzles employed in the industry are much bigger than used in lab-scale equipment. Nijdam and Langrish[72] and Fyfe et al.[73] also reported similar results with the final particle size produced from a laboratory-scale co-current spray dryer to be in the order of 20 µm while it was bigger for the commercially produced skim milk powder.

The distribution of the recovered particle sizes examined under SEM is presented in Figure 16. Irrespective of the particle size, they all have wrinkled or shriveled morphology. Both et al.[74] revealed that such morphologies are typical for small droplets (20-100 µm) and low TS content. Also, other researchers[73,75–77] reported similar findings for droplets with low TS. The appearance of broken or shattered particles in the images can be attributed to the overpressure effects created within the particles owing to the high gas outlet temperature making the particle shell to burst and break.[72]

5. Conclusions

An experimental investigation of skim milk spray drying in a counter-current configuration was conducted in a novel lab-scale dryer. The effects of process parameters: air inlet temperature, airflow rate, and feed flow rate on the temperature profiles in the dryer were studied in detail. In order to assess the atomization quality, the droplet size and velocity data were obtained for different nozzle orifices and liquid viscosities at different pressures using the PDIA technique. Water was used initially as feed material to quantify the process parameters on the drying performance, followed by experiments with skim milk drying.

The results showed that maximum evaporation rates in the dryer are obtained at the highest air inlet temperature of 360 °C, while significant impingement of water droplets was observed at a low air inlet temperature of 260 °C. The influence of airflow rate did not have a significant effect except at a very low airflow rate of 300 kg/h. Atomization was found as the key factor that controls the evaporation zones and the maximum temperature drop in the dryer. At low feed rates (17–19 kg/h), maximum evaporation occurred in the top of the dryer, while at higher feed rates (23–28 kg/h), due to the greater droplet velocities, the lowest temperature zone is shifted downstream of the dryer.

Investigations conducted on the skim milk drying showed an analogy to the water tests. Moreover, the small droplets/particles were prone to deposition and sticking to the walls. This was associated with the low glass transition temperatures of small particles. Additionally, two deposition zones were identified, a top zone where dried particles were found sticking on the walls due to the high air temperatures and a bottom zone where due to higher particle moisture content and low air temperatures, semi-dried deposits were observed.

The recovered skim milk particles exhibited typical wrinkled morphology attributed to the low solid content and small droplet sizes. Furthermore, under fixed airflow conditions, the obtained product had a similar final particle size and moisture content for different atomization conditions.

Our results show that it is indeed possible to have a process intensified spray drying technology in a counter-current setup using an elevated air temperature of 260–360 °C. The main challenge and current bottleneck for the high-temperature milk spray drying in a small volume is the accommodation and control of various size droplets with different velocities and drying rates, and the separation of such droplets/particles before they impinge the walls. The areas where the maximum droplets impact are identified as the top and the bottom of the dryer. The introduction of swirling flows at these locations should, however, reduce the problem.

Acknowledgements

This research is conducted within the project RMD-Radial Multizone Dryer (DR-20-10), in collaboration with Institute for Sustainable Process Technology (Drying and Dewatering cluster), FrieslandCampina, Energy Research Centre of the Netherlands (ECN) part of TNO and Université Catholique de Louvain. Authors would like to express their gratitude to all the project members for the fruitful discussions and to Henk-Jan Moed for the technical support. The authors also gratefully acknowledge H.S. Diepeveen for his support in the experiments.

Funding

The project is co-funded by TKI-Energy with the supplementary grant 'TKI- Toeslag' for Topconsortia for Knowledge and Innovation (TKI's) of the Ministry of Economic Affairs and Climate Policy.

References

[1] OECD-FAO. "Outlook for milk production growth" [Internet]. Paris; **2012**. DOI: 10.1787/agr_outlook-2012-graph96-en.

[2] FAO. The future of food and agriculture [Internet]. **2009**. http://www.fao.org/3/a-i6583e.pdf.

[3] Masters, K. *Spray Drying Handbook*; George Godwin Ltd: London, UK, **1985**, pp 668.

[4] Mujumdar, A. S. *Handbook of Industrial Drying*, 3rd ed.; CRC press: Boca Raton; **2006**, pp 1312.

[5] Bellinghausen R. Spray Drying from Yesterday to Tomorrow: An Industrial Perspective. *Drying Technol.* **2018**, *37*(5), 612–622.

[6] Woo, M. W.; Bhandari, B. Spray Drying for Food Powder Production. In *Handbook of Food Powders*, Bhandari, B., Bansal, N., Zhang, M., Schuck, P., Eds.; Cambridge, UK: Woodhead Publishing limited, 2013; pp 29–56. doi: 10.1533/9780857098672.1.29

[7] Huang, X.; Sormoli, M. E.; Langrish, T. A. G. Review of Some Common Commercial and Noncommercial Lab-Scale Spray Dryers and Preliminary Tests for a Prototype New Spray Dryer. *Drying Technol.* **2018**, *36*, 1900–1912. [cited 2019 Jun 6]. https://www.tandfonline.com/action/journalInformation?journalCode=ldrt20. DOI: 10.1080/07373937.2018.1459679.

[8] Kudra, T.; Mujumdar, A. S. *Advanced Drying Technologies*, 2nd ed.; CRC press: Boca Raton; **2009**, pp 480.

[9] Zbicinski, I.; Piatkowski, M. Continuous and Discrete Phase Behavior in Countercurrent Spray Drying Process. *Drying Technol.* **2009**, *27*(12), 1353–1362. doi: 10.1080/07373930903383661

[10] Ali, M.; Mahmud, T.; Heggs, P. J.; Ghadiri, M.; Bayly, A.; Ahmadian, H.; Martin de Juan, L. CFD Modeling of a Pilot-Scale Countercurrent Spray Drying Tower for the Manufacture of Detergent Powder. *Drying Technol.* **2017**, *35*, 281–299. [cited 2020 Apr 22]. https://www.tandfonline.com/action/journalInformation?journalCode=ldrt20. DOI: 10.1080/07373937.2016.1163576.

[11] Huntington, D. H. The Influence of the Spray Drying Process on Product Properties. *Drying Technol.* **2004**, *22*(6), 1261–1287. doi: 10.1081/DRT-120038730

[12] Wawrzyniak, P.; Jaskulski, M.; Piatkowski, M.; Sobulska, M.; Zbicinski, I.; Egan, S. Experimental Detergent Drying Analysis in a Counter-Current Spray Dryer with Swirling Air Flow. *Drying Technol.* **2020**, *38*, 108–116. DOI: 10.1080/07373937.2019.1626878.

[13] Ali, M.; Mahmud, T.; Heggs, P. J.; Ghadiri, M.; Djurdjevic, D.; Ahmadian, H.; de Juan, L. M.; Amador, C.; Bayly, A. A One-Dimensional Plug-Flow Model of a Counter-Current Spray Drying Tower. *Chem. Eng. Res. Des.* **2014**, *92*(5), 826–841. doi: 10.1016/j.cherd.2013.08.010.

[14] Jubaer, H.; Xiao, J.; Chen, X. D.; Selomulya, C.; Woo, M. W. Identification of Regions in a Spray Dryer Susceptible to Forced Agglomeration by CFD Simulations. *Powder Technol.* **2019**, *346*, 23–37. DOI: 10.1016/j.powtec.2019.01.088.

[15] Razmi, R.; Yu, W.; Young, B.; Woo, M. W. What Is Important in the Design of Counter Current Spray Drying Towers?. In *Chemeca 2019: Chemical Engineering Megatrends and Elements*; Engineers Australia: Sydney, Australia, 2019; pp. 5–15.

[16] Shakiba, S.; Mansouri, S.; Selomulya, C.; Woo, M. W. In-Situ Crystallization of Particles in a Counter-Current Spray Dryer. *Adv. Powder Technol.* **2016**, *27*, 2299–2307. DOI: 10.1016/j.apt.2016.07.001.

[17] Moejes, S. N.; Visser, Q.; Bitter, J. H.; Van Boxtel, A. J. B. Closed-Loop Spray Drying Solutions for Energy Efficient Powder Production. *Innov. Food Sci. Emerg. Technol.* **2018**, *47*, 24–37. doi: 10.1016/j.ifset.2018.01.005.

[18] Langrish, T. A. G.; Fletcher, D. F. Spray Drying of Food Ingredients and Applications of CFD in Spray Drying. *Chem. Eng. Process. Process Intensif.* **2001**, *40*(4), 345–354. doi: 10.1016/S0255-2701(01)00113-1

[19] Benali, M.; Kudra, T. Process Intensification for Drying and Dewatering. *Drying Technol.* **2010**, *28*(10), 1127–1135. doi: 10.1080/07373937.2010.502604

[20] Benali, M.; Kudra, T. *Drying Process Intensification: Application to Food Processing*, 2008. Available at: https://www.researchgate.net/publication/266211018 (accessed Nov 11, 2018).

[21] Comission, E. **2015** low-carbon economy [Internet]; **2016**. https://www-europarl-europa-eu.ezproxy2.utwente.nl/RegData/docs_autres_institutions/commission_europeenne/com/2016/0500/COM_COM(2016)0500_EN.pdf.

[22] Creative Energy. European Roadmap for Process Intensification. Creative Energy. European Roadmap for Process Intensificatio [Internet]. The Netherlands; **2008** [cited 2021 Jul 16]. http://www.creative-energy.org.

[23] Frydman, A.; Vasseur, J.; Ducept, F.; Sionneau, M.; Moureh, J. Simulation of Spray Drying in Superheated Steam Using Computational Fluid Dynamics. *Drying Technol.* **1999**, *17*, 1313–1326. DOI: 10.1080/07373939908917617.

[24] Frydman, A.; Vasseur, J.; Moureh, J.; Sionneau, M.; Tharrault, P. Comparison of Superheated Steam and Air Operated Spray Dryers Using Computational Fluid Dynamics. *Drying Technol.* **1998**, *16*, 1305–1338. [cited 2019 Jan 11]. http://www.tandfonline.com/action/journalInformation?journalCode=ldrt20. DOI: 10.1080/07373939808917464.

[25] Linke T.; Happe, J.; Kohlus, R. Laboratory-Scale Superheated Steam Spray Drying of Food and Dairy Products. *Drying Technol.* **2021**, 1–12. doi: 10.1080/07373937.2020.1870127

[26] Lum, A.; Cardamone, N.; Beliavski, R.; Mansouri, S.; Hapgood, K.; Woo, M. W. Unusual Drying Behaviour of Droplets Containing Organic and Inorganic Solutes in Superheated Steam. *J. Food Eng.* **2019**, *244*, 64–72. DOI: 10.1016/j.jfoodeng.2018.09.021.

[27] ISPT. RMZD-Radial Multizone Dryer [Internet]; **2018**. https://ispt.eu/media/Project-Poster-DR-20-10-RMD-Radial-Multizone-Dryer.pdf.

[28] topsetor energie. NL. Radial Multi-zone Dryer [Internet]; **2018**. https://projecten.topsectorenergie.nl/storage/app/exports/project-radial-multi-zone-dryer-00033042-1609692962.pdf.

[29] De Wilde, J.; de Broqueville, A. Rotating Fluidized Beds in a Static Geometry: Experimental Proof of Concept. *AIChE J.* **2007**, 53(4), 793–810. doi: 10.1002/aic.11139.

[30] De Wilde, J. Gas-Solid Fluidized Beds in Vortex Chambers. *Chem. Eng. Process* **2014**, *85*, 256–290. DOI: 10.1016/j.cep.2014.08.013.

[31] Broqueville, A. d.; De Wilde, J.; Tourneur, T. Device for Treating Particles in a Rotating Fluidized Bed [Internet]. The Netherlands; WO/2018/203745; **2018**. https://patentscope.wipo.int/search/en/detail.jsf?docId=WO2018203745.

[32] Tourneur, T.; De Broqueville, A.; Sweere, A.; Poortinga, A.; Wemmers, A.; Jamil Ur Rahman, U.; et al. **2019**. *Experimental and Numerical Study of a Radial Multi-Zone Vortex Chamber Spray Dryer*. Florence, Italy.

[33] Weber, J. M.; Stehle, R. C.; Breault, R. W.; De Wilde, J. Experimental Study of the Application of Rotating Fluidized Beds to Particle Separation. *Powder Technol.*, 2017, *316*, 123–130. doi: 10.1016/j.powtec.2016.12.076.

[34] Jamil Ur Rahman, U.; Pozarlik, A. K.; Tourneur, T.; de Broqueville, A.; De Wilde, J.; Brem, G. Numerical Study toward Optimization of Spray Drying in a Novel Radial Multizone Dryer. *Energies*, 2021, *14*(5). doi: 10.3390/en14051233.

[35] Kieviet, F. G.; Kerkhof, P. J. A. M. Air Flow, Temperature and Humidity Patterns in a Co-Current Spray Dryer: Modelling and Measurements. *Drying Technol.* 1997, *15*(6–8), 1763–1773. doi: 10.1080/07373939708917325.

[36] Francia, V.; Martín, L.; Bayly, A. E.; Simmons, M. J. H. Agglomeration in Counter-Current Spray Drying Towers. Part A: Particle Growth and the Effect of Nozzle Height. *Powder Technol.* **2016**, *301*, 1330–1343. DOI: 10.1016/j.powtec.2016.05.011.

[37] Atuonwu, J. C.; Stapley, A. G. F. Reducing Energy Consumption in Spray Drying by Monodisperse Droplet Generation: Modelling and Simulation. *Energy Procedia*, **2017**, *123*, 235–242. doi: 10.1016/j.egypro.2017.07.251.

[38] van Deventer, H.; Houben, R.; Koldeweij, R. New Atomization Nozzle for Spray Drying. *Drying Technol.* **2013**, *31*, 891–897. Jun 11 [cited 2019 Oct 17]. DOI: 10.1080/07373937.2012.735734.

[39] Jaskulski, M.; Tran, T. T. H.; Tsotsas, E. Design Study of Printer Nozzle Spray Dryer by Computational Fluid Dynamics Modeling. *Drying Technol.* **2020**, *38*, 211–223. DOI: 10.1080/07373937.2019.1633541.

[40] Fischer, C.; Jaskulski, M.; Tsotsas, E. Inline Method of Droplet and Particle Size Distribution Analysis in Dilute Disperse Systems. *Adv. Powder Technol.* **2017**, *28*, 2820–2829. DOI: 10.1016/j.apt.2017.08.009.

[41] Moejes, S. N.; van Boxtel, A. J. B. Energy Saving Potential of Emerging Technologies in Milk Powder Production. *Trends Food Sci. Technol.*, **2017**, *60*, 31–42. doi: 10.1016/j.tifs.2016.10.023.

[42] Kota, K.; Langrish, T. A. G. Fluxes and Patterns of Wall Deposits for Skim Milk in a Pilot-Scale Spray Dryer. *Drying Technol.* 2006, *24*(8), 993–1001. doi: 10.1080/07373930600776167.

[43] Ozmen, L.; Langrish, T. A. G. An Experimental Investigation of the Wall Deposition of Milk Powder in a Pilot-Scale Spray Dryer. *Drying Technol.* 2003, *21*(7), 1253–1272. doi: 10.1081/DRT-120023179.

[44] Langrish, T. A. G. G.; Chan, W. C.; Kota, K. Comparison of Maltodextrin and Skim Milk Wall Deposition Rates in a Pilot-Scale Spray Dryer. *Powder Technol.* **2007**, *179*, 84–89. DOI: 10.1016/j.powtec.2007.01.019.

[45] Gianfrancesco, A.; Turchiuli, C.; Dumoulin, E.; Palzer, S. Prediction of Powder Stickiness Along Spray Drying Process in Relation to Agglomeration. *Part. Sci. Technol.* 2009, *27*(5), 415–427. doi: 10.1080/02726350903129987.

[46] Gianfrancesco, A.; Turchiuli, C.; Dumoulin, E. Powder Agglomeration During the Spray-Drying Process: Measurements of Air Properties. *Dairy Sci. Technol.* 2008, *88*(1), 53–64. doi: 10.1051/dst:2007008.

[47] Sadripour, M.; Rahimi, A.; Hatamipour, M. S. Experimental Study and CFD Modeling of Wall Deposition in a Spray Dryer. *Drying Technol.* **2012**, *30*, 574–582. [cited 2018 Oct 1]. http://www.tandfonline.com/action/journalInformation?journalCode=ldrt20. DOI: 10.1080/07373937.2011.653613.

[48] Kim, K. S.; Kim, S.-S. Drop Sizing and Depth-of-Field Correction in TV Imaging. *At. Sprays*, 1994, *4*(1).

[49] Lee, S. Y.; Kim, Y. D. Sizing of Spray Particles Using Image Processing Technique. *KSME Int. J.*, 2004, *18*(6), 879–894.

[50] Castrejón-García, R.; Castrejón-Pita, J. R.; Martin, G. D.; Hutchings, I. M. The Shadowgraph Imaging Technique and Its Modern Application to Fluid Jets and Drops. *Revista Mexicana Física.* 2011, *57*(3), 266–275.

[51] Sinha, A.; Surya Prakash, R.; Madan Mohan, A.; Ravikrishna, R. V. Airblast Spray in Crossflow - Structure, Trajectory and Droplet Sizing. *Int. J. Multiphase Flow* **2015**, *72*, 97–111. 1DOI: 10.1016/j.ijmultiphaseflow.2015.02.008.

[52] Sallevelt, J. L. H. P.; Pozarlik, A. K.; Brem, G. Characterization of Viscous Biofuel Sprays Using Digital Imaging in the near Field Region. *Appl. Energy* **2015**, *147*, 161–175. DOI: 10.1016/j.apenergy.2015.01.128.

[53] Meijer, R. *Atomization of Viscous Newtonian Fluids Using Pressure Swirl Atomizers: An experimental approach using Particle/Droplet Image Analysis for the quantification of spray characteristics* [Unpublished master's thesis]. University of Twente, the Netherlands, 2019.

[54] Adamczyk, A. A.; Rimai, L. 2-Dimensional Particle Tracking Velocimetry (PTV): Technique and Image Processing Algorithms. **1988**, *6*, 373–380.

[55] Patterson, H. S.; Cawood, W. The Determination of Size Distribution in Smokes. *Trans. Faraday Soc.* **1936**, *32*, 1084–1088. doi: 10.1039/TF9363201084.

[56] Sallevelt, J. L. H. P.; Pozarlik, A. K.; Beran, M.; Axelsson, L.-U.; Brem, G. Bioethanol Combustion in An Industrial Gas Turbine Combustor: Simulations and Experiments. *J. Eng. Gas Turbines Power.* 2014, *136*(7), 071501. doi: 10.1115/1.4026529.

[57] Mandato, S.; Rondet, E.; Delaplace, G.; Barkouti, A.; Galet, L.; Accart, P.; Ruiz, T.; Cuq, B. Liquids' Atomization with Two Different Nozzles: Modeling

of the Effects of Some Processing and Formulation Conditions by Dimensional Analysis. *Powder Technol.* **2012**, *224*, 323–330. doi: 10.1016/j.powtec.2012.03.014.

[58] Glycerine Producers' Association and G. P. Association. *Physical properties of glycerine and its solutions*. Glycerine Producers' Association: New York, 1963.

[59] Klaassen, M. (2016). Near Filed Atomization in Pressure Swirl Nozzle: Experimental Investigation regarding Impact of Fluid Properties and Nozzle Specifications on Spray Characteristics [Unpublished master's thesis]. University of Twente, the Netherlands.

[60] Gourdon, M.; Innings, F.; Jongsma, A.; Vamling, L. Qualitative Investigation of the Flow Behaviour during Falling Film Evaporation of a Dairy Product. **2015**, *60*, 9–19.

[61] Silveira, A. C. P.; de Carvalho, A. F.; Perrone, Í. T.; Fromont, L.; Méjean, S.; Tanguy, G.; Jeantet, R.; Schuck, P. Pilot-Scale Investigation of Effectiveness of Evaporation of Skim Milk Compared to Water. *Dairy Sci. & Technol.* **2013**, *93*, 537–549. JulDOI: 10.1007/s13594-013-0138-1.

[62] Rahman, U. J. U.; Baiazitov, I.; Pozarlik, A. K.; Brem, G. CFD Study of Air Flow Patterns and Droplet Trajectories in a Vortex Chamber Spray dryer. In *Proceedings of the 21st International Drying Symposium,* Valencia, Spain, 11–14 September **2018**.

[63] Rahman, U. J. U.; Pozarlik, A. K.; Baiazitov, I.; Tourneur, T.; de Broqueville, A.; De Wilde, J.; Brem, G. Stationary and Transient Aspects of Air Flow in a Novel Radial Multi-Zone Dryer. In *Proceedings of the Euro Drying*, Torino, Italy, 10–12 July 2019.

[64] Tourneur, T.; de Broqueville, A.; De Wilde, J. Experimental and CFD study of multi-zone vortex chamber spray dryers," in *International Symposium on Chemical Reactor Engineering-ISCRE 25*, **2018**, vol. 25. https://www.aidic.it/iscre25/review/papers/407tourneur.pdf (accessed Aug. 20, 2018).

[65] Lefebvre, A. H.; McDonell, V. G. *Atomization and Sprays*; CRC press; **2017**.

[66] Davanlou, A.; Lee, J. D.; Basu, S.; R. Kumar. Effect of Viscosity and Surface Tension on Breakup and Coalescence of Bicomponent Sprays. *Chem. Eng. Sci.* **2015**, 131, 243–255. doi: 10.1016/j.ces.2015.03.057.

[67] Ranz, W. E.; Marshall, W. R., Jr. Evaporation from Drops. *Chem. Eng. Prog. I and II.* 1952, *48*, 141–146, 173–180.

[68] Vuataz, G. The Phase Diagram of Milk: A New Tool for Optimising the Drying Process. *Le Lait*, **2002**, *82*(4), 485–500. doi: 10.1051/lait:2002026.

[69] Walmsley, T. G.; Walmsley, M. R. W.; Atkins, M. J.; Neale, J. R.; Sellers, C. M. An Experimentally Validated Criterion for Skim Milk Powder Deposition on Stainless Steel Surfaces. *J. Food Eng.* **2014**, *127*, 111–119. [cited 2018 Sep 28]. DOI: 10.1016/j.jfoodeng.2013.11.025.

[70] O'Donoghue, L. T.; Haque, M. K.; Kennedy, D.; Laffir, F. R.; Hogan, S. A.; O'Mahony, J. A.; Murphy, E. G. Influence of Particle Size on the Physicochemical Properties and Stickiness of Dairy Powders. *Int. Dairy J.* **2019**, *98*, 54–63. doi: 10.1016/j.idairyj.2019.07.002.

[71] Ullum, T.; Sloth, J.; Brask, A.; Wahlberg, M. Predicting Spray Dryer Deposits by CFD and an Empirical Drying Model. *Drying Technol.* **2010**, *28*, 723–729. [cited 2018 Oct 1]. http://www.tandfonline.com/action/journalInformation?journalCode=ldrt20. DOI: 10.1080/07373931003799319.

[72] Nijdam, J. J.; Langrish, T. A. G. An Investigation of Milk Powders Produced by a Laboratory-Scale Spray Dryer. *Drying Technol.* 2005, *23*(5), 1043–1056. doi: 10.1081/DRT-200060208.

[73] Fyfe, K.; Kravchuk, O.; Nguyen, A. V.; Deeth, H.; Bhandari, B. Influence of Dryer Type on Surface Characteristics of Milk Powders. *Drying Technol.* **2011**, *29*, 758–769. DOI: 10.1080/07373937.2010.538481.

[74] Both, E. M.; Boom, R. M.; Schutyser, M. A. I. Particle Morphology and Powder Properties during Spray Drying of Maltodextrin and Whey Protein Mixtures. *Powder Technol.* **2020**, *363*, 519–524. [cited 2021 Jan 11]. DOI: 10.1016/j.powtec.2020.01.001.

[75] Wu, W. D.; Liu, W.; Gengenbach, T.; Woo, M. W.; Selomulya, C.; Chen, X. D.; Weeks, M. Towards Spray Drying of High Solids Dairy Liquid: Effects of Feed Solid Content on Particle Structure and Functionality. *J. Food Eng.* **2014**, *123*, 130–135. [cited 2018 Sep 18]. DOI: 10.1016/j.jfoodeng.2013.05.013.

[76] Rogers, S.; Wu, W. D.; Lin, S. X. Q.; Chen, X. D. Particle Shrinkage and Morphology of Milk Powder Made with a Monodisperse Spray Dryer. *Biochem. Eng. J.* **2012**, *62*, 92–100. DOI: 10.1016/j.bej.2011.11.002.

[77] Langrish, T. A. G.; Marquez, N.; Kota, K. An Investigation and Quantitative Assessment of Particle Shape in Milk Powders from a Laboratory-Scale Spray Dryer. *Drying Technol.* **2006**, *24*(12), 1619–1630. doi: 10.1080/07373930601031133.